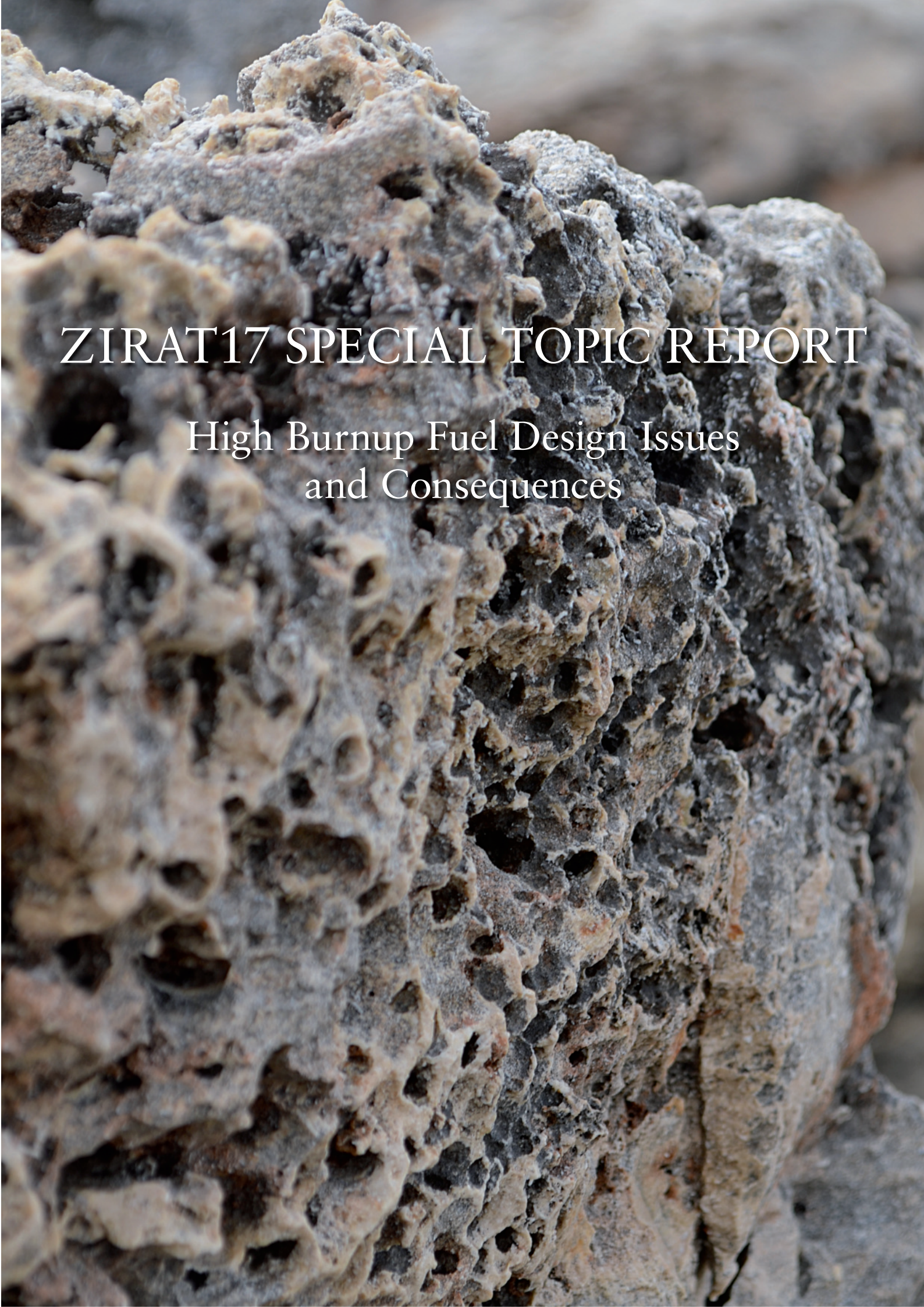

ZIRAT17 SPECIAL TOPIC REPORT

High Burnup Fuel Design Issues and Consequences

High Burnup Fuel Design Issues and Consequences

Authors

Peter Rudling
ANT International, Mölnlycke, Sweden

Charles Patterson
Clovis, CA, USA

Ron Adamson
Fremont, CA, USA

Friedrich Garzarolli
Fürth, Germany

Alfred Strasser
Sleepy Hollow, NY, USA

Tony Turnbull
Bristol, UK

Technical Editor

Peter Rudling
ANT International, Mölnlycke, Sweden

Reviewer

Charles Patterson
Clovis, CA, USA

A.N.T. INTERNATIONAL®

Advanced Nuclear Technology International
Analysvägen 5, SE-435 33 Mölnlycke
Sweden

info@antinternational.com
www.antinternational.com

Ecolabelled printed matter, 441 799

Disclaimer

The information presented in this report has been compiled and analysed by Advanced Nuclear Technology International Europe AB (ANT International®) and its subcontractors. ANT International has exercised due diligence in this work, but does not warrant the accuracy or completeness of the information. ANT International does not assume any responsibility for any consequences as a result of the use of the information for any party, except a warranty for reasonable technical skill, which is limited to the amount paid for this assignment by each ZIRAT/IZNA programme member.

Contents

1 Introduction

One of the major present challenges to nuclear energy lies in its commercial competitiveness. To stay competitive, the industry needs to maximize the availability and capacity factors of nuclear power plants while reducing maintenance and fuel cycle costs and enhancing safety. In the absence of large scale reprocessing and recycling and the lack of permanent repositories, the industry also needs to manage used nuclear fuel in a safe, efficient and cost effective manner. Extended burnup is one of the methods applied to meet these objectives. There are a number of issues related to normal operation, anticipated operation occurrences, design basis accidents and dry storage that need resolution to be able to successfully implement extended burnup. This special topic reviews the potential consequences of increased burnup on fuel. Recommendations are also given on how to remedy the high burnup issues.

The Report structure is as follows:

- Section 2 provides background information on water reactors and their fuel,
- Section 3 discusses burnup trends and general issues related to extended burnup,
- Section 4 reviews issues related to increased burnup and reactor safety, fuel design and operation,
- Section 5 presents conclusions while
- Section 6 contains recommendations on how to resolve the issues.

Related information is given in FMTR Vol. 1 [Cox et al, 2006] and FMTR Vol. 2 [Rudling et al, 2007], as well as the following ZIRconium Alloy Technology (ZIRAT)/International Atomic Energy Agency (IZNA) Special Topic Reports (STR):

Corrosion and hydriding topics:

- Hydriding Mechanisms and Impact on Fuel Performance, ZIRAT5/IZNA1 [Cox & Rudling, 2000].
- Corrosion of Zirconium Alloys, ZIRAT7/IZNA2 [Adamson et al, 2002/2003].
- Corrosion of Zr-Nb Alloys in PWRs, ZIRAT9/IZNA4 [Cox et al, 2004/2005].
- Corrosion mechanisms, ZIRAT12/IZNA7 [Adamson et al, 2007/2008].
- Impact of Water Chemistry and Chalk River Unidentified Deposits (CRUD) on Fuel Performance, ZIRAT6/IZNA1 [Wikmark & Cox, 2001/2002].
- The Effects of Zn Injection (PWRs and BWRs) and Noble Metal Chemistry (BWRs) on Fuel Performance, ZIRAT8/IZNA3 [Cox et al, 2003/2004].

Thermal and mechanical property topics:

- Mechanical Properties of Zirconium Alloys, ZIRAT6/IZNA1 [Adamson & Rudling, 2001/2002].
- Pellet Cladding Interaction and Pellet Cladding Mechanical Interaction, ZIRAT11/IZNA6 [Adamson et al, 2006/2007b].
- Processes Going on in Nonfailed Rod During Normal Operation, ZIRAT15/IZNA10 [Patterson & Garzarolli, 2010].
- Processes Going on in Nonfailed Rod During Accident Conditions (LOCA and RIA), ZIRAT15/IZNA10 [Strasser et al, 2010b].

Fuel performance topics:

- Dimensional Instability, ZIRAT7/IZNA2 [Adamson & Rudling, 2002/2003].
- High Burnup Fuel Issues – Their Most Recent Status, ZIRAT8/IZNA3 [Adamson et al, 2003/2004].
- Structural Behaviour of Fuel Components, ZIRAT10/IZNA5 [Cox et al, 2005/2006].
- Impact of Irradiation on Material Performance, ZIRAT10/IZNA5 [Adamson & Cox, 2005/2006].

☐Other relevant topics:

- Manufacturing of Zirconium Alloy Materials, ZIRAT5/IZNA1 [Rudling & Adamson, 2000].
- Manufacturing of Zr-Nb alloys, ZIRAT11/IZNA6 [Nikulina et al, 2006/2007].
- Welding of Zirconium Alloys, ZIRAT12/IZNA7 [Rudling et al, 2007/2008].

2 Reactor and fuel assembly characteristics

2.1 General

There is a wide range of environments in which LWR fuel is operated. Table 2-1 shows typical ranges of various parameters.

Table 2-1: Design Parameters for water cooled reactors, after [Adamson et al, 2002/2003].

Parameter	Western type PWR	VVER (440/1000) MW	CANDU[1]	BWR	RBMK[2]
1. Coolant	Pressurized H_2O	Pressurized H_2O	Pressurized D_2O	Boiling H_2O	Boiling H_2O
2. Fuel Materials (Pressure tube materials)	Zry-4, ZIRLO, DUPLEX, M5, Inconel, SS[3]	Zr-alloy E110	Zry-4 (Zr2.5Nb)	Zry-2, Zry-4, Inconel, SS	Zr-alloy E110, (Zr2.5Nb)
3. Average power rating, (kW/l)	80-125	83/108	9-19	40-57	5
4. Fast Neutron Flux, Average, n/cm².s	6-9E13	5E13/7E13	1.5-2E12	4-7E13	1-2E13
5. Temperatures, °C					
Average Coolant inlet	279-294	267/290	249-257	272-278	270
Average Coolant outlet	313-329	298/320	293-305	280-300	284
Max Cladding OD	320-350	335/352	310	285-305	290
Steam mass content, %				7-14	14
6. System pressure, bar	155-158	125/165	96	70	67
7. Coolant Flow, m/s	3-6*	3.5/6	3-5	2-5*	3.7
8. Coolant Chemistry**					
Oxygen, ppb	<0.05	<0.1		200-400	<20
Hydrogen (D_2), ppm	2-4		(3-10)	.05-.30	-
cc/kg	25-50	30-60			
Boron (as Boric acid), ppm	0-2200	0-1400	-	-	-
Li (as LiOH), ppm	0.5-6.0	0.05-0.6	1	-	-
K (as KOH), ppm	-	5-20		-	-
NH_3, ppm		6-30			
NaOH, ppm		0.03-0.35			

*Variation from lower to upper part of the core and from plant to plant.
**Zn in ppb quantities may be added for BWRs and PWRs; Pt and Rh in ppb quantities may be added for BWRs.

[1]Canadian Deuterium Uranium (CANDU), [2]Reaktor Bolshoi Mozhnosti Kanalov (RBMK), [3]Stainless Steel (SS), [4]Voda Voda Energo Reactor (VVER), [5]Zirconium Low Oxidation (ZIRLO)

ANT International, 2012

There is a wide variety of different types of fuel assemblies for LWRs described more in the following subsections.

2.2 BWRs

The fuel rod array for BWRs was initially 7x7 but there has been a trend over the years to increase the number of rods so that now most fuel assemblies are either of 9x9 or 10x10 square configuration designs. An example of a BWR fuel assembly based on a 10x10 lattice is shown in Figure 2-1. The driving force in the trend toward larger number of fuel rods in each fuel assembly was the reduction of Linear Heat Generation Rate (LHGR). Such changes which resulted in a number of fuel performance benefits such as lower Fission Gas Release (FGR) and increased PCI margins. However, to decrease fuel cycle costs, the LHGRs of 9x9 and 10x10 fuel assemblies have successively been increased so that peak heat generation rates are today almost comparable to those of the older 7x7 and 8x8 designs.

In all BWRs, fuel bundles are enclosed in open-ended, square tubes or "channels". The combination of a fuel bundle (rods, spacers, tie plates and related hardware) and a channel is commonly identified as a fuel assembly. The channels are ducts for coolant flow that prevent lateral flow of coolant among the assemblies operating at different power levels. They also form the inter-assembly space into which control blades are inserted.

Fuel assemblies are positioned in a reactor core support structures at the bottom and top of each assembly. Lower tie or bottom support plates (as in Figure 2-1) are supported by a pedestal that carries the assembly weight and directs coolant into the channel. The upper ends of fuel assemblies are supported laterally by a rectangular lattice structure which bears against wear pads on the outer surface of the fuel channels. Cruciform-shaped control blades are located in the region between the channels of selected sets of four fuel assemblies. Part of the incoming coolant is diverted into the region among fuel assemblies to transfer heat from the control blades and prevent boiling.

Irrespective of the many possible different shapes, sizes and configurations, the common fuel assembly design requirements are:

- Maintain proper positioning of the fuel rods under normal operating conditions and in Design Basis Accidents (DBAs); i.e., maintain a controllable and coolable (safe) geometry during normal operation, anticipated operating occurrences and during postulated seismic events, LOCA, RIA.
- Contain or at least confine fuel materials and fission products
- Facilitate handling before and after irradiation.

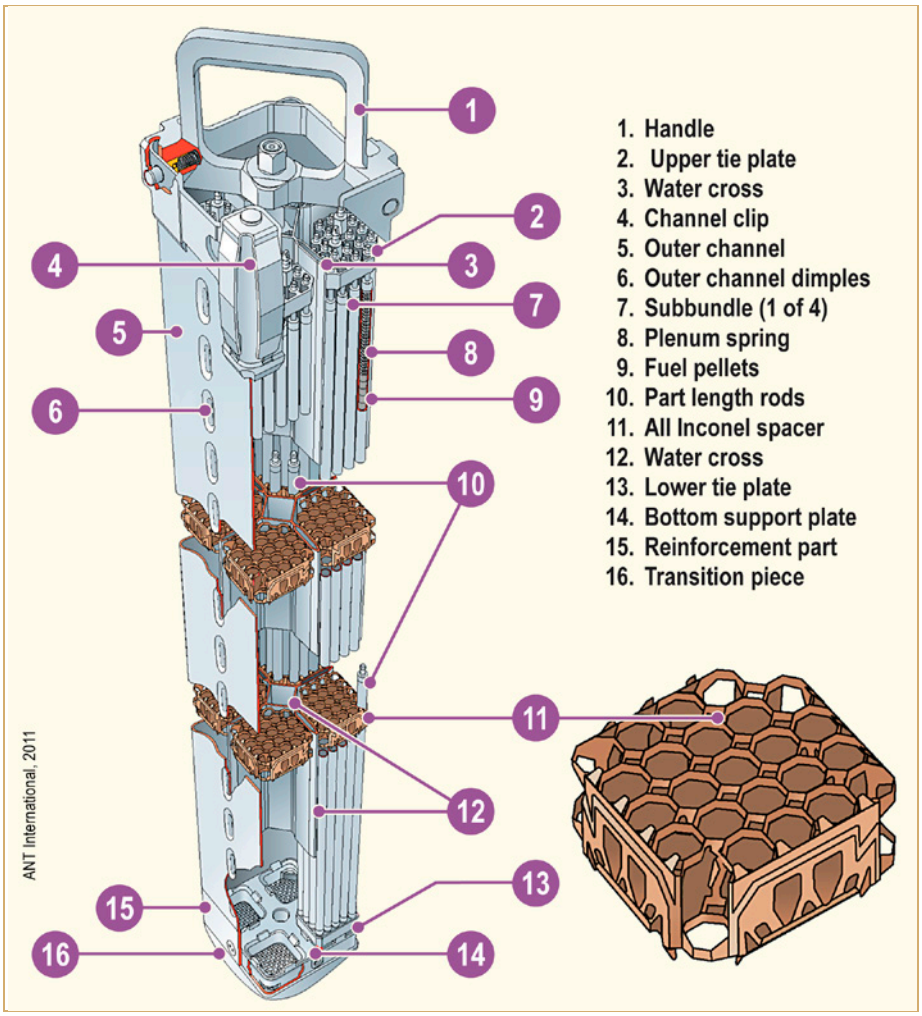

Figure 2-1: The BWR Fuel SVEA-96 Optima2, provided by the courtesy of Westinghouse Electric.

2.3 PWRs

Also for PWRs there has been a trend to greater subdivision of fuel rods, e.g. from W 15x15 to 17x17 design. However, since PWRs do not have the same flexibility with core internals and control rods as BWRs, to accomplish this requires modified reactor internals. There is however, one exception namely DC Cook 1 which is switching to 17x17 by changing the reactor internals. Figure 2-2 shows the current PWR fuel rod arrays.

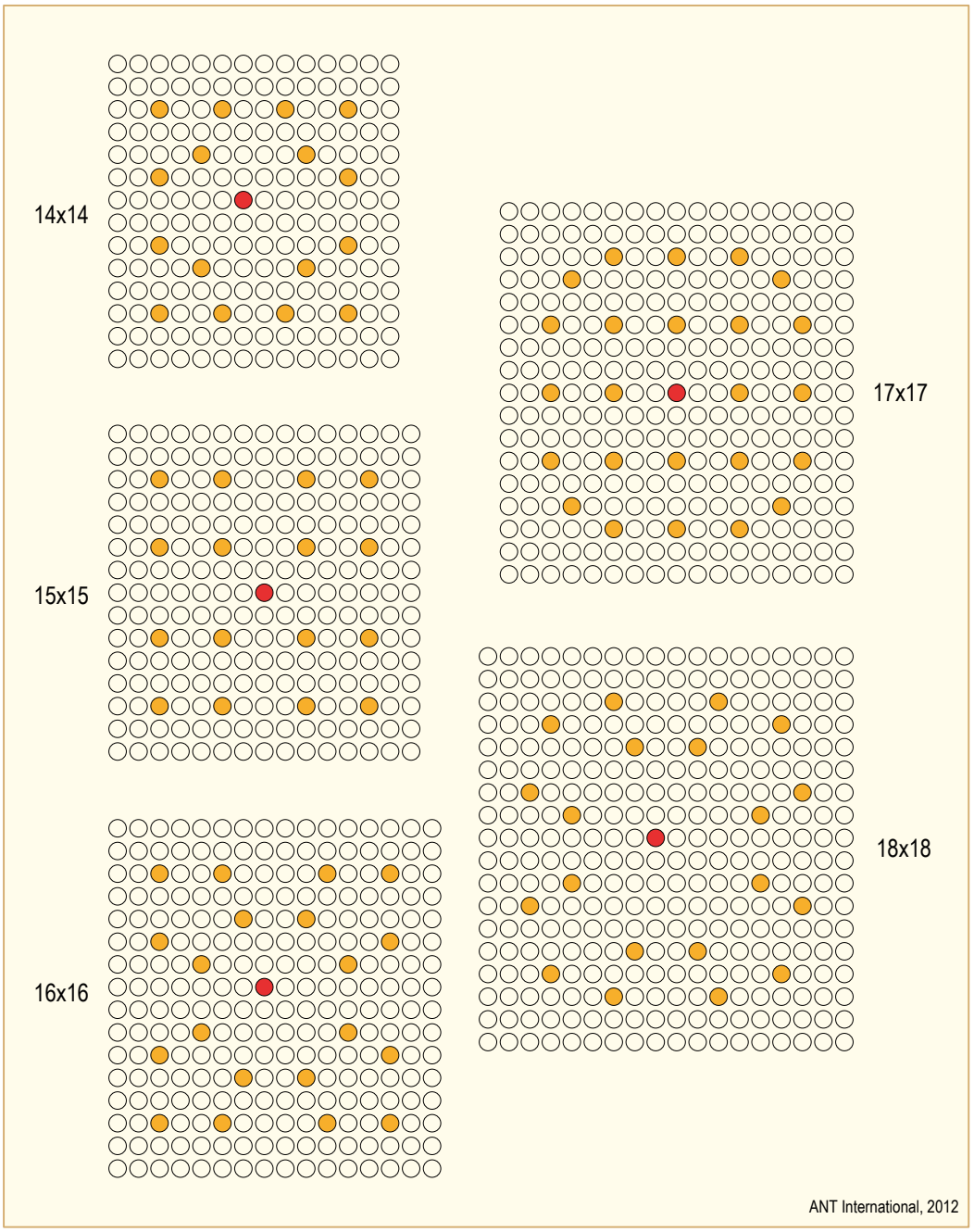

Figure 2-2: Layouts of different PWR fuel assembly arrays. Rods marked with yellow colour are GTs into which the control rod cluster is inserted. The position marked by a red filled circle is the IT position.

In most PWRs, the assemblies are positioned in the core by bottom and top fittings, and the lateral clearances are restricted by the assembly-to-assembly contacts at the spacer-grid levels. PWR control rods consist of Rod Cluster Control Assemblies, RCCAs, the poison part of which moves into guide thimbles (or GTs). These guide thimbles are an integral part of the assembly structure.

As an example of a PWR fuel design, the High Thermal Performance (HTP) design (former Siemens design) is shown in Figure 2-3. The unique feature of HTP grid concept is that the fuel rods are supported along four pairs of continuous lines, providing a large grid-to-rod contact surface with coolant mixing being affected by curved internal flow channels. The HTP mid span mixing grid has no contact between the grid and the fuel rod. These grids are only used to improve thermal-hydraulic performance. The FUELGUARD bottom nozzle design (Figure 2-4), was originally designed for HTP fuel but can be used for all designs as a means for preventing debris from entering a fuel assembly with the reactor coolant.

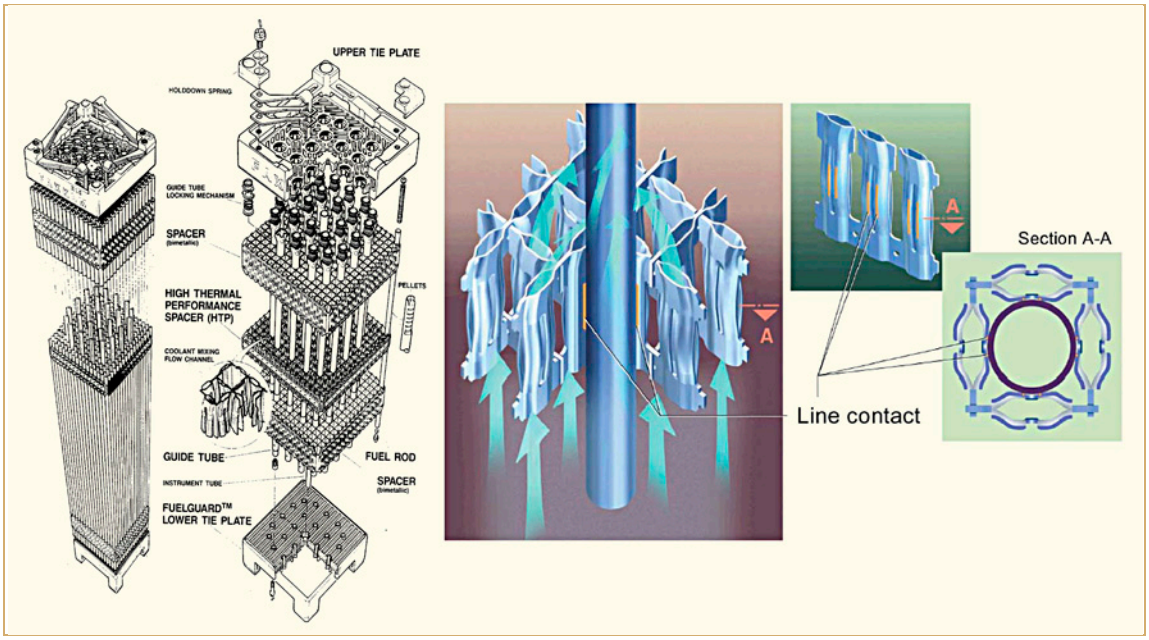

Figure 2-3: AREVA NP PWR HTP 17 x 17- HTP spacer grid design [Baleon et al, 2001].

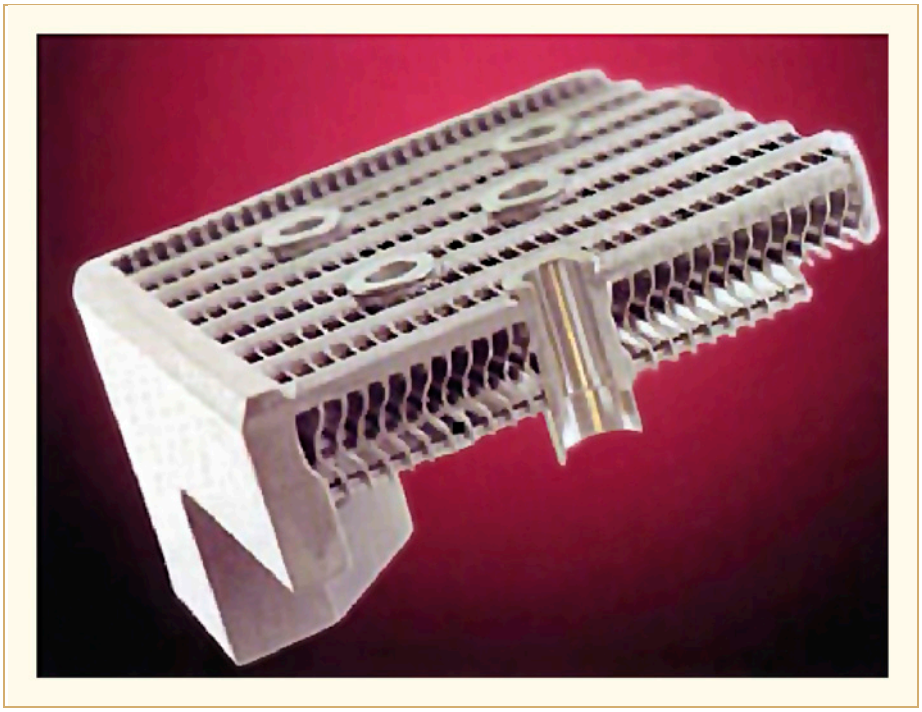

Figure 2-4: FUELGUARD bottom nozzle, provided by the courtesy of AREVA NP.

2.4 CANDU

The CANDU reactor is a heavy water moderated and cooled natural uranium fuelled reactor in which the fuel bundles (50 cm long and usually 12 per fuel channel) are contained in individual pressure tubes through which the heavy water coolant flows. The number of pressure tubes varies according to the power output of the reactor (e.g. 380 in the CANDU-6 design). Reactor outlet temperatures vary somewhat, but are typically in the range of 310-315°C. The pressure tubes are separated from the "cold" (60-80°C) heavy water moderator contained in a large, horizontal, cylindrical Calandria Vessel. Each individual Calandria Tube in the Calandria Vessel contains a smaller diameter Pressure Tube. The Calandria and pressure tubes are separated by an insulating gas gap which is maintained by spacers ("Garter Springs"). There were initially 2 spacers per pressure tube, but this was increased to 4 per tube in all reactors after the failure of the G8 pressure tube in Pickering-2 as a result of the pressure tube sagging into contact with the calandria tube [Hart, 1997].

A simplified diagram of the Calandria Vessel, end shields and fuel channels is shown in Figure 2-5.

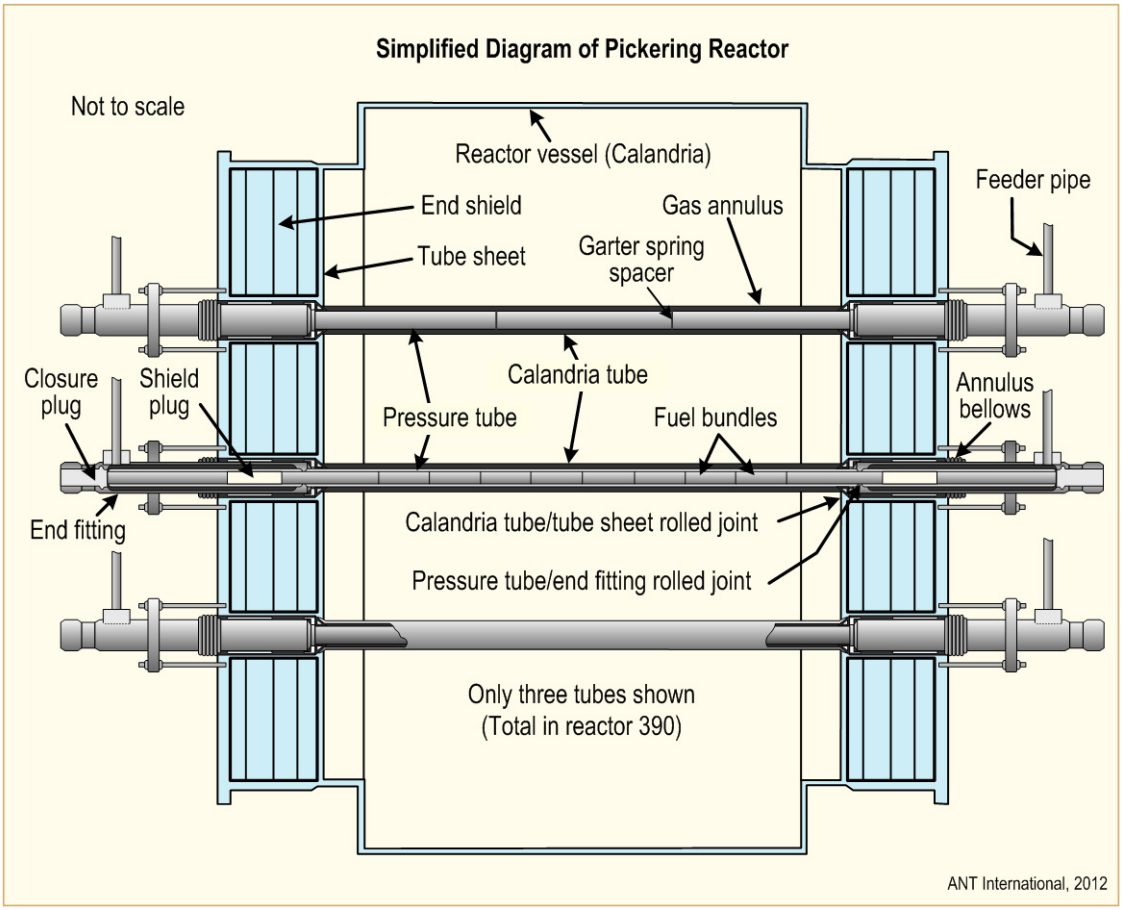

Figure 2-5: Simplified diagram of Pickering reactor showing fuel channels and garter springs.

Details of an individual fuel channel showing the end fittings that the fuelling machines latch onto during on-power refuelling operations are shown in Figure 2-6. The typical appearance of the pressure tube-calandria tube spacers (garter springs) is shown in Figure 2-7. These garter springs were initially of Zr-2.5Nb-0.5Cu alloy, and were a tight fit on the pressure tube. They were subsequently changed to a loose fit, which allowed vibrations to cause spacers to move out of place during reactor construction. This movement was a major contributor to the P2-G8 pressure tube failure. A subsequent change to tight fitting Inconel 728 spacers (4 in number) resulted from this event. The gas annulus between the pressure tube and the calandria tube was initially filled with nitrogen, but this was changed to carbon dioxide to reduce deuterium uptake in the pressure tube from deuterium diffusing into the gas annulus from the stainless steel end fitting.

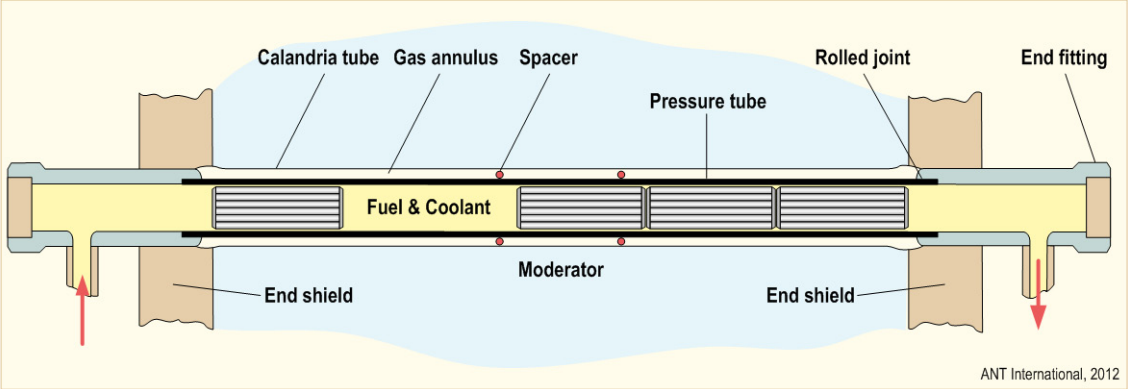

Figure 2-6: Schematic of a fuel channel for a CANDU reactor with pressurized water coolant.

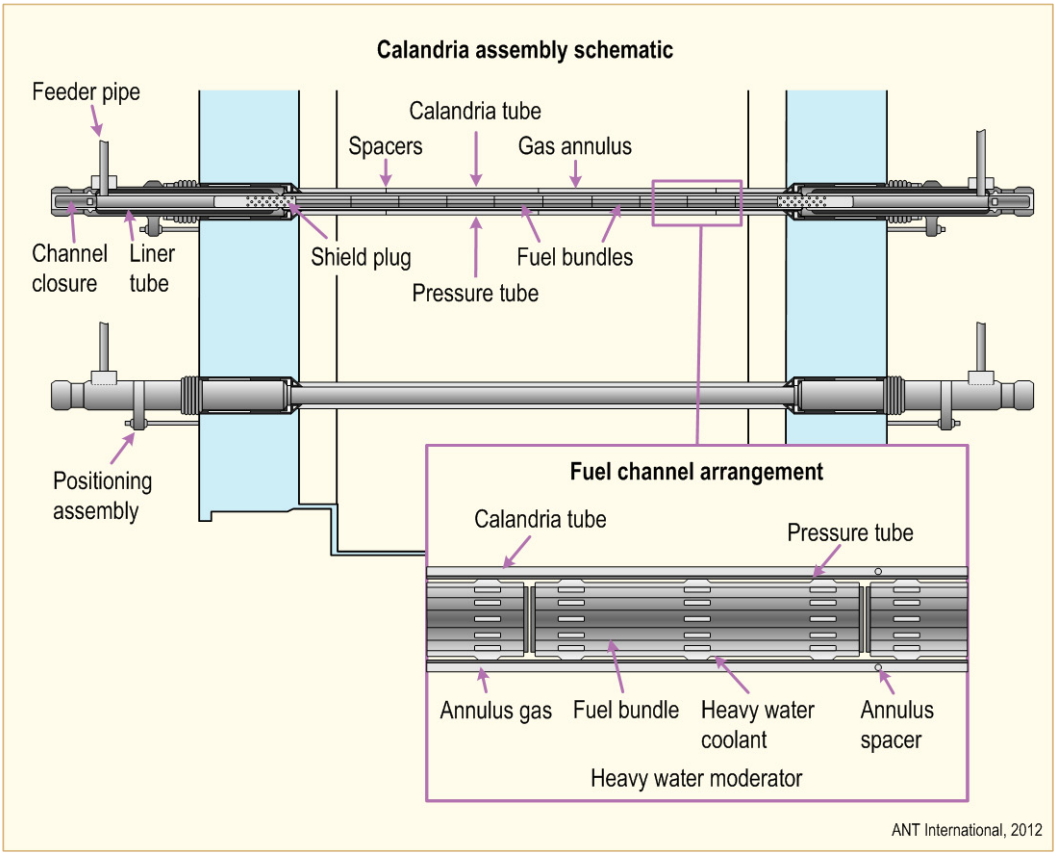

Figure 2-7: "Garter spring" spacer assembly, showing the locations of the four spacers now standard on all pressure tubes.

3 Burnup trends

3.1 Introduction

"Burnup" is defined as the total energy released per initial unit mass of fuel as a result of irradiation. Commonly used units are megawatt days per metric ton of uranium (MWd/MTU). Burnup in commercial light water reactors is also commonly expressed in terms of gigawatt days per metric ton of uranium (GWd/MTU) or, equivalently, megawatt days per kilogram of uranium (MWd/kgU). When dealing with MOX fuel, burnup is frequently expressed in terms of initial heavy metal or simply metal (MWd/kgM) of or the same in gigawatt days (GWd/MT). Occasionally, burnup is expressed in terms atomic depletion or fissions per initial atom (%).

The major incentive for extended burnup is the potentially improved fuel cycle economy. Economic analyses in past ZIRAT/IZNA reports indicated that economic incentives for extending BUs beyond the 60-70 GWD/MT batch average range will disappear and that other incentives must exist in order to justify going beyond the economically optimal level. The improved economics depend in part on the decreased amount of fuel to be purchased and to be stored and recycled or disposed after irradiation. This is balanced by the increased amount of uranium and enrichment services required. The economics of decreased assemblies could also be impacted by the much longer cooling times required for high burnup and Mixed Oxide (MOX) fuels in spent fuel pools prior to on-site dry storage or transport to a storage facility as noted later. The economic analyses are also dependent on the utility's accounting systems and as a result are utility and even plant specific.

The average batch burnup at discharge from US PWRs are currently in the range of 42-54 GWD/MT and from US BWRs in the range of 45-52 GWD/MT. The average assembly burnup within a batch is about 43 GWD/MT for PWRs and 48 GWD/MT for BWRs shown as a function of time in Figure 3-1. The PWRs have levelled off and the BWRs are still increasing slightly, approaching the Nuclear Regulatory Commission (NRC) regulatory limit of 62.5 GWD/MT peak rod.

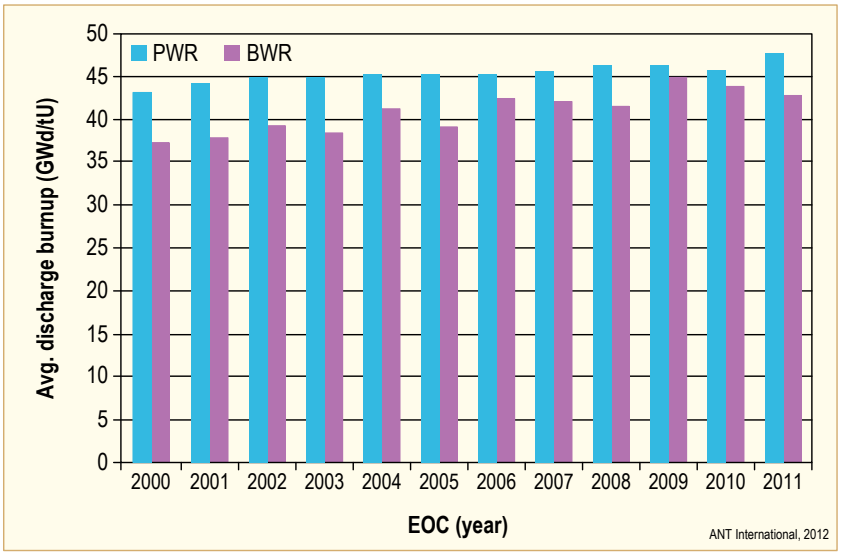

Figure 3-1: Average US discharged assembly BU trends, after [Daum, 2011].

Some European plants have operated in the batch average burnup range of 50-60 GWD/MT and are preparing to operate to 62 GWD/MT in their current cycles in both PWRs and BWRs. This is feasible, in part, due to their greater margin to their regulatory burnup limits in comparison with US plants. The maximum burnup Lead Test Assemblies (LTAs) are in the range of 67-79 GWD/MT for both PWRs and BWRs. Burnup ranges by countries are compared to their regulatory limits in Table 3-1.

In addition to potential technical issues, described in later sections, the two major constraints to achieving higher burnup are the regulatory limits noted in Table 3-1 and the 5% limit on ^{235}U enrichment. The regulatory limits are set to ensure sufficient margins towards the fuel design criteria described in Section 4.3.

Table 3-1: Maximum burnups achieved vs. regulatory limits, (excluding LTAs), Strasser in [Adamson et al, 2011].

Vendor	Design	PWR	Design	BWR
AREVA (Framatome)	AFA3G Mark B-12, 15x15 Mark BW[9], 17x17 Mark BW, x1 (LTA) CE HTP[10], 14x14 FOCUS HTP Dx[11]D4, HTP M5 DX-ELS [12]0.8	68 assy (M5) 58 assy (Zry-4) 50 assy 52 assy, 58 rod 68 assy, 72 rod 48 assy 58 batch, 60 assy 57-60 batch, 58-60 assy	ATRIUM 10XM ATRIUM 10XL ATRIUM 10XP	53 batch, 57 assy., 64 rod 30 rod 54 batch, 60 assy., 62 rod
GNF			GE[13]12 GE14 GNF2	50 batch, 68 assy. 52 batch, 72 assy. 10 batch, 43 assy.
W	ZIRLO[14] { OFA. 17x17 Std, 17x17 V, 14x14 opt. ZIRLO, NGF[15] (LTA) RFA[16]-2	56 batch, 68 assy. 48 assy. 52 assy. 63 assy. 49 batch, 55 assy., 60 rods 68 assy., (LTA)	Optima 2	57 batch, 60 assy.
TVEL[17]	TVA, TVS[18] TVS-2	58 assy. 48 assy.		
				ANT International, 2011

3.2 Fuel design changes to reach higher burnups

Increased reactivity needed for higher burnup introduces local peaking and control issues that can affect T-H operation via DNB or CPR and CHF. Such issues can arise due to differences in local power peaking early life when reactivity is high and when fuel assemblies with high and low reactivities are located in close proximity.

[9] Basket-Weave
[10] High Thermal Performance
[11] Duplex
[12] Duplex Extra-Low Sn
[13] General Electric
[14] ZIRconium Low Oxidation
[15] Next Generation Fuel
[16] Robust Fuel Assembly
[17] Russian Fuel Vendor
[18] Name of one of TVEL fuel designs

4 Fuel performance issues related to increased burnup

4.1 Overview

Issues related to fuel cycles and ultimate burnup capabilities were discussed in the earlier section. Issues related directly to fuel performance are discussed in this section. Fuel performance issues relate primarily to the integrity of fuel assemblies, their ability to perform safely at elevated burnup and the effects of extended exposure on the transportation of spent nuclear fuel and the back end of the fuel cycle. The fuel itself is expected to change with burnup according to existing models. These changes must be addressed in design, licensing and operation, but are not expected to involve precipitous breakdowns in properties or behaviour that could prevent further increases in burnup. Cladding corrosion, hydrogen pickup and their effects on cladding behaviour during normal and accident conditions and during dry storage become increasingly important with increasing burnup. Cladding issues have led to the development of new alloys for extended exposures in PWRs and appear to be leading to the refinement of alloys for BWRs as well. Extended exposures are also expected to affect some structural components of fuel assemblies and the behaviour of integral fuel assemblies; e.g., spacer grids and springs, bowing and control rod interference. These issues are reviewed in the following notes.

4.2 Basic impact of irradiation on fuel materials

4.2.1 Introduction

During irradiation, the thermal, mechanical and chemical conditions in a fuel rod vary with power, exposure or time and operating history. The temperature of the fuel follows an approximately parabolic distribution across the pellet radius and varies strongly with power. It also varies with the thermal conductance of the pellet-to-cladding gap, the cladding itself, the oxide, CRUD and water films on the outside surface of the cladding and with the bulk coolant temperature. Nearly all of these factors change with burnup to degrade heat transfer and increase local temperature at a given heat generation rate.

Early life is characterized by the transfer of heat across the gas-filled gap between pellets and cladding, which almost universally contains helium. Early life also involves a number of processes that affect thermal and structural conditions in the rod; e.g.:

- Fracture of the fuel pellets due to thermal stresses starting on the first rise to power and continuing during the initial 5-10 GWd/MTU according to power and power history.
- Radial relocation of fuel fragments toward the inner cladding surface.
- Pellet densification, which is typically small in modern fuel.
- Depending on the pellet manufacturing process, the evolution of a small amount of volatiles.

Continued irradiation leads to other changes on the inside of a fuel rod; e.g.:

- Fission gas release (FGR) from fuel pellets to the free volume within a fuel rod, with increasing gas pressure inside the fuel rod and decreasing thermal conductivity of the helium filler gas due to the addition of krypton and xenon.
- Solid and gaseous fuel pellet swelling due to the accumulation of fission products and the formation of bubbles and other gas filled voids.
- Inward cladding creep due to temperature, fast neutron flux and the net difference between internal gas and external coolant pressures.
- Increasing amounts of pellet-cladding mechanical interaction due to gap closure by radial relocation, pellet swelling, inward cladding creep and differential thermal expansion between pellets and cladding.

- Healing of the cracks among pellet fragments by in situ sintering to a degree that depends on operating conditions and history.
- Hot pressing[22] and the formation of dishes on the ends of flat pellets or filling of dishes, which were formed during pellet fabrication.
- The release of fission products with the potential for contributing to cladding failure by processes such as Stress Corrosion Cracking (SCC);i.e. iodine or liquid metal embrittlement (LME); i.e., cadmium with caesium.

At moderate to high exposures, the chemistry of the fuel changes in a manner which can affect its thermal and mechanical properties. An example is an increase in the pellet oxygen-to-metal ratio leading to a decrease in thermal conductivity, increases in pellet temperature and increases in pellet creep rates. With sufficient contact at the pellet-cladding interface, temperature and time, oxygen can also be transferred from the fuel pellets to the cladding.

On the outer surface of a fuel rod, exposure, time, temperature or combinations of these factors lead to oxidation of the cladding and deposition of corrosion products (CRUD) from reactor internals and piping. Surface corrosion reduces the thickness of the cladding wall and leads to the pickup of hydrogen in the cladding metal. Wall thinning is typically small in modern zirconium-based cladding, but is addressed in the design process and is identified as a key factor in postulated LOCAs. Hydrogen pickup leads to concentrations in the cladding that increase with exposure or time. Hydrogen concentrations normally exceed the solubility limit at operating temperatures by low-to-moderate burnups in most zirconium alloys. Hydrogen concentrations in excess of the solubility limit lead the precipitation of hydrides. Such hydrides are brittle relative to the matrix of zirconium-based cladding. At sufficiently large concentrations, hydrides can degrade the ductility and fracture toughness of the cladding. The embrittlement effects of the hydrides depend on temperature, hydride distribution and orientation in relation to the main tensile stress direction. The density of soluble hydrogen and insoluble zirconium hydride is lower than that of zirconium, so that hydrogen pickup and hydride precipitation produce strains in the cladding and other Zr-alloy components, such as guide tubes and channels. With increasing hydride concentrations, the combination of low ductility and local strains can cause structural failure at the location of hydride blisters, lenses or sunbursts. Based on experience in Japanese power and test reactors, hydrogen and hydrides have also been implicated in an outside-in cladding cracking process in relation to a power ramp.

Nickel base alloys used in spacers/grids change their properties due to neutron irradiation, as follows: (1) a hardening, (2) an increase of the sensitivity to intercrystalline stress corrosion cracking (ISCC), and (3) to a relaxation of stress due to irradiation creep. The last aspect is of most concern because it is an important parameter for an adequate rod support within the spacers, adequate fuel assembly hold-down and adequate bypass flow.

The processes that take place in the fuel rod during in-reactor operation are interrelated in a highly non-linear manner. The principal processes and their interactions are shown schematically in Figure 4-1 and Figure 4-2. Most of these processes stem from fissioning, heat generation and elevated temperatures. They factor into a set of constraints that defines the conditions under which fuel is operated. As shown in Figure 4-3, these constraints vary with exposure such that physical limits at high burnup are due primarily to decreasing (nuclear) reactivity, cladding lift-off (discussed in Section 4.4.1.7) and hydride-induced degradation of cladding properties so as to create regulatory concerns regarding fuel behaviour and safety margins, particularly under the conditions of postulated accidents. As shown in Figure 4-4, these constraints lead to a set of design and operating margins which start with fundamental safety concerns and propagate through to the manner in which fuel is operated.

[22] Hot pressing involves closure of pellet pores by hydrostatic pressure. It can be considered stress-assisted densification and is the opposite of gaseous swelling (discussed later).

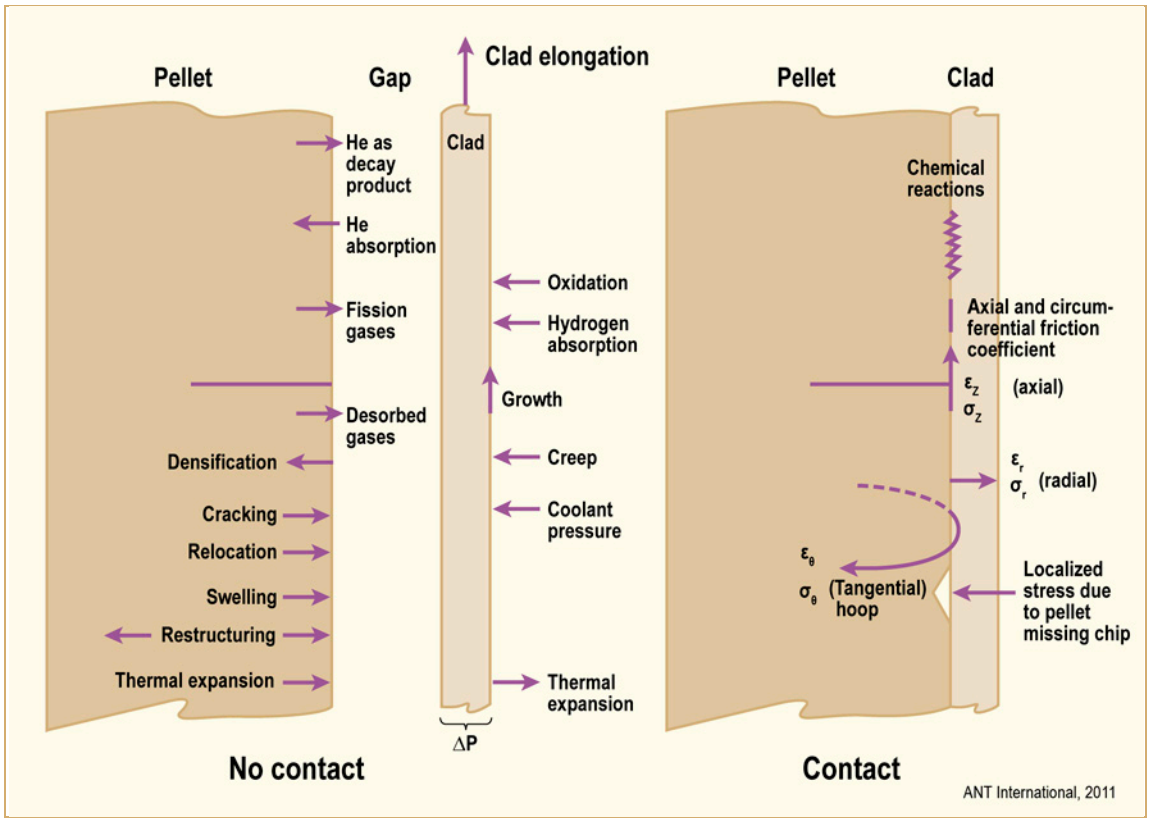

Figure 4-1: Schematic showing the different processes occurring in the FR during irradiation for open and closed gap conditions, after [Strasser et al, 2010a].

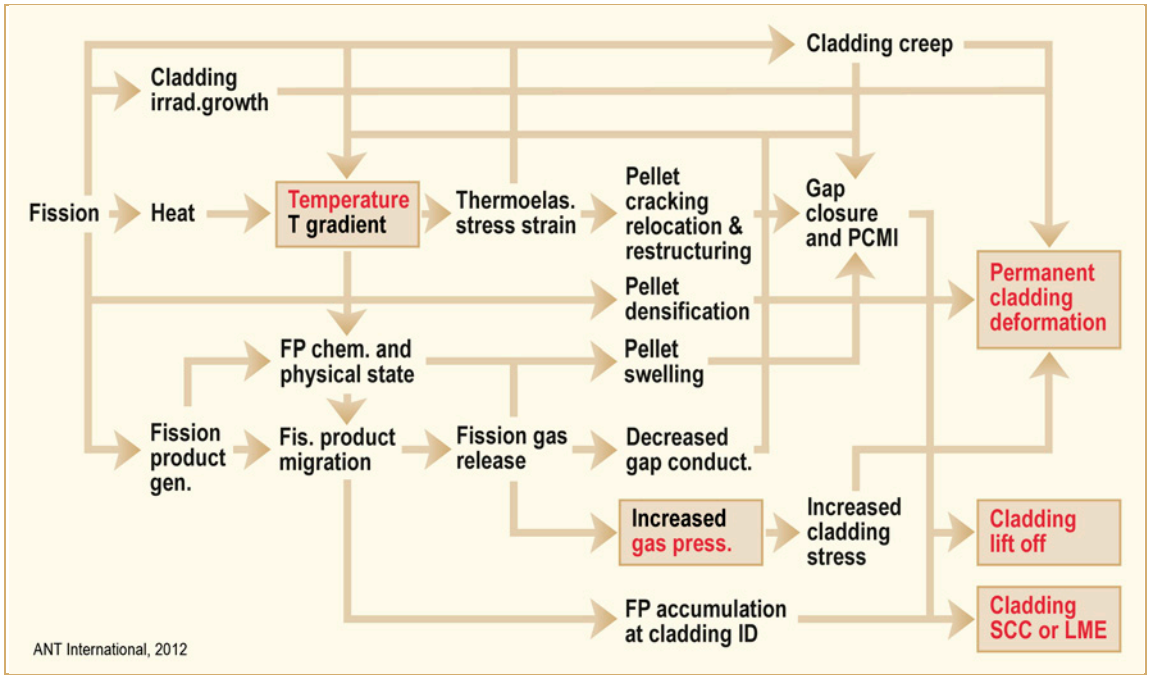

Figure 4-2: Interaction among processes within an operating fuel rod. Key design criteria are enclosed with a box and shown in red, after [Mohr et al, 1976].

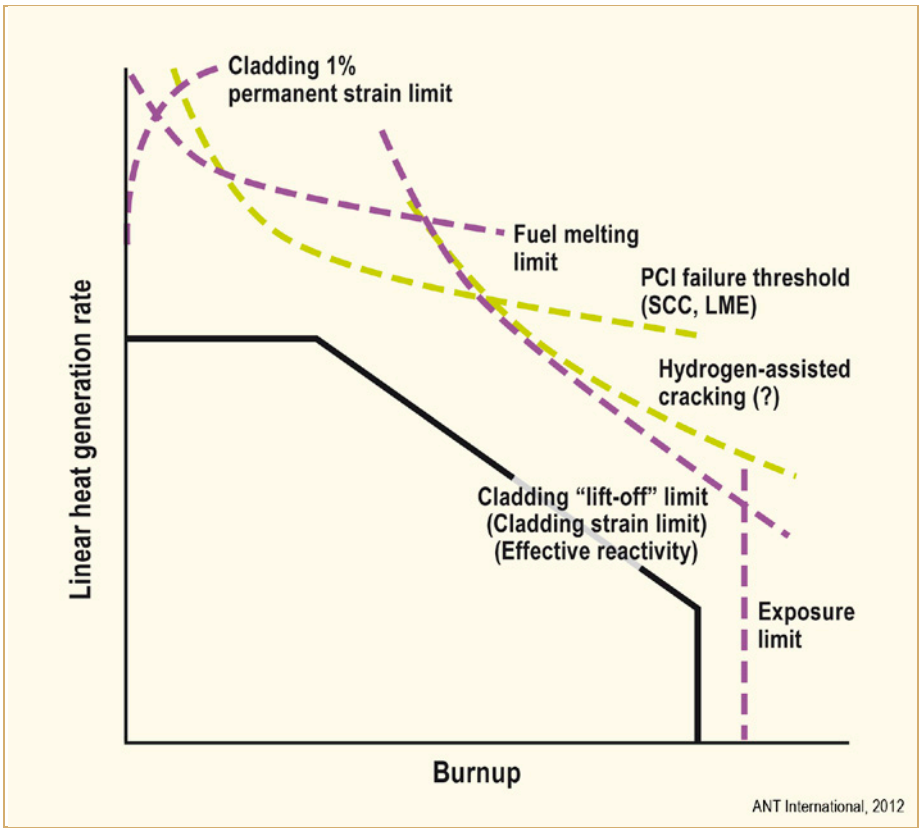

Figure 4-3: Schematic diagram of fuel rod heat generation and design constraints relative to burnup, (after MATPRO and FRAPCON, after [Hagrman, 1993]).

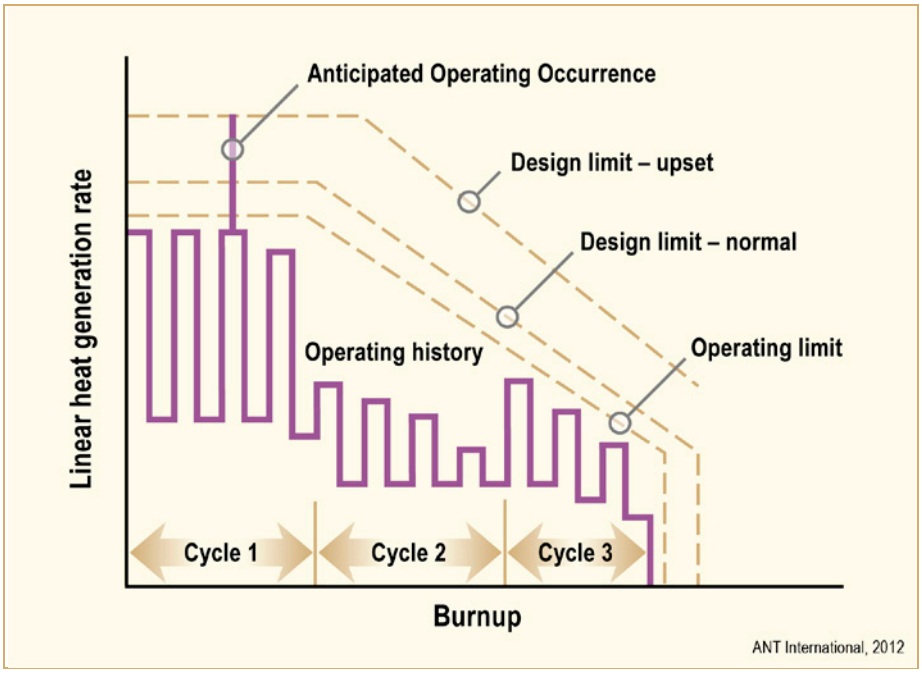

Figure 4-4: Schematic diagram of power-exposure operating envelope and related margins, after [Patterson, 2012].

4.2.2 Fuel pellet

4.2.2.1 Introduction

The properties and behaviour of fuel pellets evolve throughout the operating life of a fuel rod. As discussed in a later section on interim storage of spent nuclear fuel, certain aspects also continue to evolve after discharge from a reactor. The first area of interest relative to high burnup is the change in effective reactivity due to depletion of the initial inventory of ^{235}U, the conversion of ^{238}U to ^{239}Pu and the accumulation of fission products. The next areas of interest are burnup-dependent changes in the thermal and mechanical properties and behaviour of fuel pellets and their effects on fuel rod performance and design margins. The general behaviour in these areas was briefly reviewed in Section 4.2.1. Additional detail is given in the following sections.

4.2.2.2 Fission process

The energy yield from fissioning varies slightly among reactor types, fuel materials and fuel designs, but is in the range of ~200 MeV/f; e.g., 202.5 MeV/f for ^{235}U and 211.5 MeV/f for ^{239}Pu [Kaye & Laby, 1995]. As a useful reference, fissioning of 1 gram of material per day produces approximately 1 megawatt of power. The majority of the fission energy, >80%, is in the form of kinetic energy of the fission fragments, which appears immediately as heat. The remaining energy is distributed among instantaneous gamma rays from excited fission fragments, kinetic energy of fission neutrons, beta particles and gamma rays from fission products and neutrinos. The energy of all except the neutrinos ultimately appears as heat. Essentially all of the neutrinos and accompanying beta particles escape due to their weak interaction with materials in a fission reactor.

When fission takes place in a fuel pellet, the excited compound nucleus formed after absorption of a neutron breaks up into two lighter nuclei, called fission fragments. Three nuclides, having sufficient stability to survive for a long time, namely, ^{233}U, ^{235}U, and ^{239}Pu, are fissionable by neutrons of all energies. Of these nuclides, ^{235}U is the only one that occurs in nature. During irradiation, ^{235}U is consumed while the fissionable materials ^{239}Pu and ^{241}Pu are produced by the capture of epithermal neutrons by ^{238}U, especially at the fuel pellet periphery. The relative rates of fissioning and isotopic concentrations in fuel initially enriched with ^{235}U are shown as functions of burnup in Figure 4-5 and Figure 4-6. By mid-life over half of the energy produced in a LWR comes from fissioning of plutonium that is converted from ^{238}U. With continued irradiation, the concentration of ^{235}U continues to decrease while the production and consumption of plutonium reaches an equilibrium state and remains relatively constant with increasing burnup. Due to the accumulation of fission products and increasing neutron absorption, the net reactivity of fuel decreases with exposure and constrains the burnup to which fuel can operate from the perspective of core management and fuel cycle economics. As discussed earlier, burnups greater than ~75 GWd/MTU in current LWRs require initial ^{235}U enrichments greater than 5%.

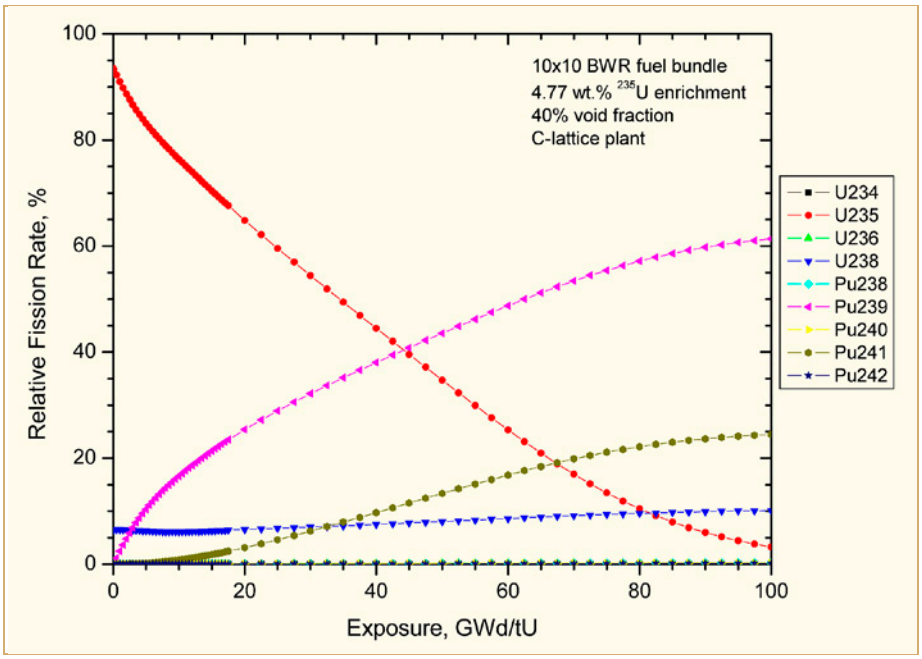

Figure 4-5: Fission rates in a BWR fuel rod relative to exposure and nuclide [Lundberg, 2010].

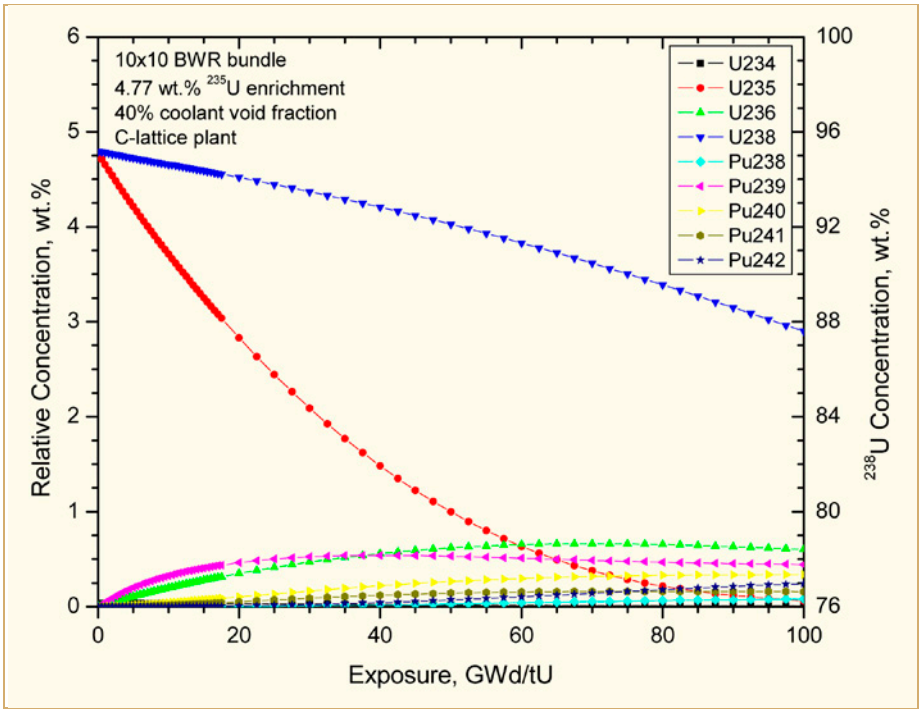

Figure 4-6: Concentration of fissile and fertile nuclides relative to exposure [Lundberg, 2010].

The fissioning and neutron capture processes are biased toward the pellet periphery because of self-shielding by ^{235}U and ^{239}Pu and by the high cross-section fission products that develop during irradiation. This bias or radial peaking varies during the course of irradiation due to changes in the fuel pellet and, in BWRs, due to changes in the neutron spectrum associated with variations in the local coolant void fraction. The predicted evolution of fissile isotopes is shown relative to radial location and burnup in Figure 4-7. This behaviour continues with irradiation and leads to a radial variation in pellet exposure at very high burnup as illustrated in Figure 4-8.

The initial ^{235}U enrichment has an effect on local pellet burnup; i.e., greater self shielding and higher surface-to-centre fissioning with higher initial enrichments. As noted above, radial peaking increases with burnup so that the fission rate is more than twice as high at the surface than that at the centre at a burnup of >40 MWd/kgU with 5% ^{235}U enrichment. The total plutonium and actinide (Np, Am, and Cm) concentration reaches about 1% and 0.08% after a burnup of 35 MWd/kgU, respectively and 1.3% and 0.016% after a burnup of 60 MWd/kgU; see [Bailly et al, 1999]. With increasing burnup, the self-shielding effect of these nuclides alters the effect of the initial ^{235}U enrichment.

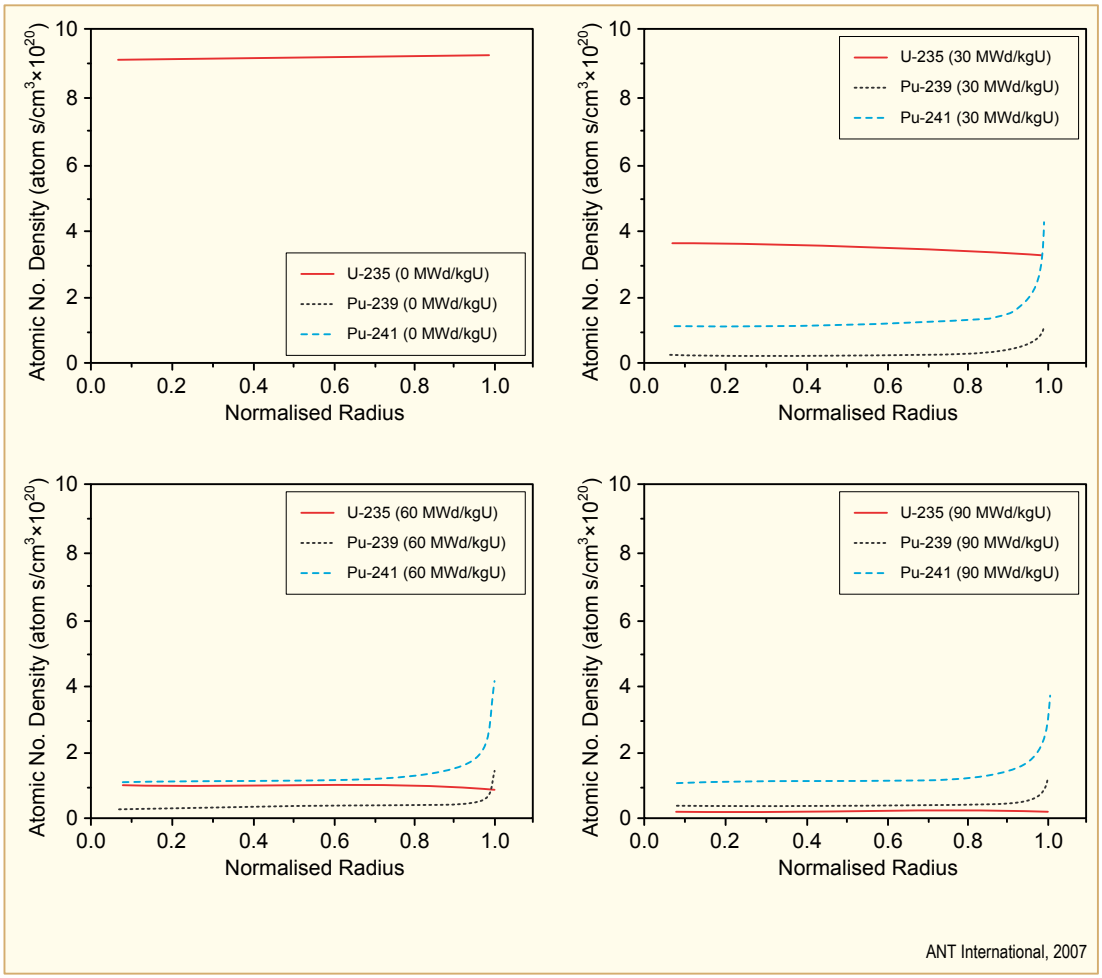

Figure 4-7: Concentration of fissile nuclides relative to radial pellet location and exposure, after [Lee et al, 2000].

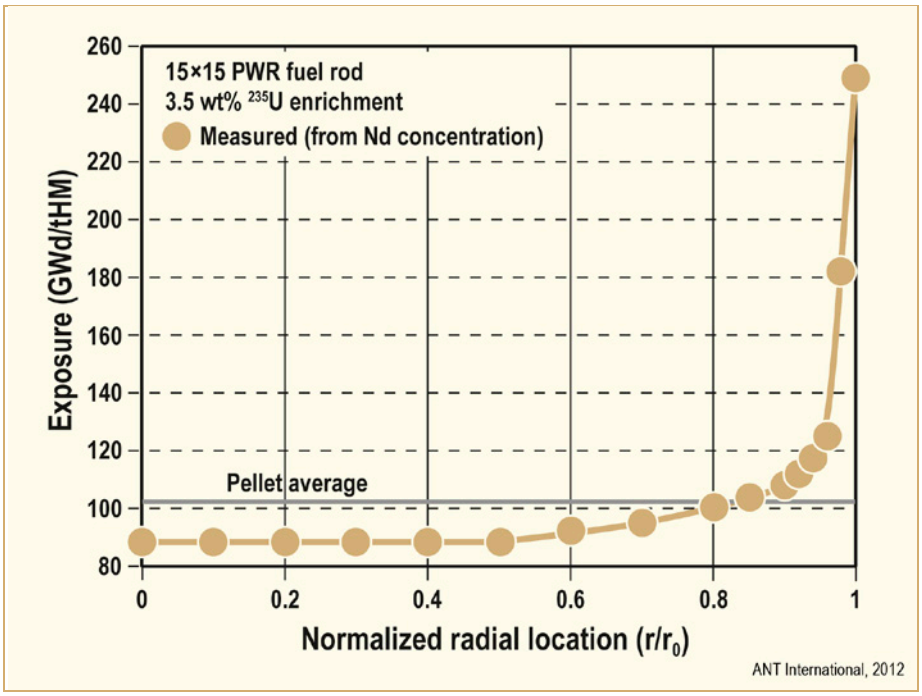

Figure 4-8: Radial exposure distribution observed at a pellet average exposure of 102 GWd/tHM, after [Walker et al, 2005].

4.2.2.3 Changes in composition with increasing burnup

The composition and structure of UO_2 and $(U,Pu)O_2$ changes during irradiation due to the generation of fission products and the manner in which they interact with the fuel matrix. About 200 stable or long-lived fission product atoms are produced within the fuel per 100 fissions. The mass numbers of most of the fission products (~94%) range from 95 to 139 and exhibit a bimodal distribution, with a "light" group centred at ~85 and a "heavy" group at ~140. The cumulative distribution or yield of fission products varies by a small amount with neutron energy (thermal vs. fast neutrons) and to a slightly larger extent with the fissioning nuclide (uranium vs. plutonium); [England & Rider, 1994]. Most of the fission products are radioactive and decay by the loss of a negative beta particle. So, the initial radionuclides transmute into ~200 fission products.

An example of the fission product production rates in a LWR rod is given in Table 4-1. These data are typical of the average, net generation rate of each nuclide during operation; i.e., μg of fission products per gm of actinide and fission products per 10 GWd/MTU. Data in this table are net inventories ≥1 ppm as calculated with the ORIGEN-2.1 computer program with operation at 18.5 kW/m core average power to 60 GWd/MTU. They represent the steady-state fission product production rates during in-reactor operation and serve as a basis for estimating fission product inventories relative to burnup.

The physical states and chemical forms vary significantly among the fission products. They are typically divided into classes based on these forms and on the effects each form has on fuel characteristics and behaviour [Olander, 1976] and [Kleykamp, 1985]. The classes are:

1) Noble gases: The noble gases Kr and Xe, which are essentially insoluble in the fuel matrix and can form either intragranular (within grain) voids of bubbles, intergranular (grain boundary) bubbles or be released from the fuel pellets to the free volume of the respective fuel rod.

2) Volatiles: Fission products with low melting temperatures and high vapour pressures (volatiles) such as bromine, rubidium, iodine, tellurium and caesium that can exist as either a gas or a solid depending on their location inside a fuel rod.

3) Metals: Metallic precipitates such as rhodium, ruthenium, technetium and some molybdenum (depending on temperature and local oxygen potential).

4) Insoluble oxides: Insoluble oxides such as barium, strontium, and some zirconium in the form of zirconates; e.g., $BaZrO_3$ and $SrZrO_3$.

5) Soluble oxides: Soluble oxides such as the rare-earth fission products, some molybdenum, niobium, yttrium, the remaining zirconium and the transuranics.

Note that helium also results from irradiation, but is not strictly a fission product. Helium is produced during and after irradiation by α-decay of actinides. The contribution of helium released from fuel pellets to the total helium inventory in the free volume of a fuel rod is small; e.g., <1% for typical UO_2 rods and 5-6% for MOX rods [Lanning et al, 2005]. Although the total production of helium during irradiation and storage due to decay is estimated to be four times the production of Kr and Xe due to fission [Ronchi & Hiernaut, 2004], the production rates and release fractions of helium during operation are small enough to have only a minor effect on the behaviour of typical LWR fuel and are neglected in some models of thermal-mechanical performance; e.g., FRAPCON-3 [Lanning et al, 2005]. Helium generation and release are potential issues for long-term storage of spent nuclear fuel and possibly for designs that are being considered to burn actinides as part of fuel recycling, but do not appear to be significant factors in the operation LWR fuel to burnups achievable with the 5% limit on ^{235}U enrichment. The effects of helium generation and extended exposures are discussed again in a later section on long-term storage.

Table 4-1: Fission generation in LWR fuel, based on ORIGEN-2.1, after [Olander, 1976] and [Kleykamp, 1985].

Fission product	Production rate wt. ppm per GWd/MTU	Notes
Noble gas		
Kr	10.9	
Xe	157.5	
Volatile		
Br	0.6	Elemental vapour or insoluble compound
Rb	10.1	Elemental vapour or insoluble oxide
Te	14.7	Elemental vapour or metallic inclusion
I	7.0	Elemental vapour of insoluble compound
Cs	84.6	Elemental vapour or insoluble oxide
Metal		
Mo	98.6	Metallic inclusion or insoluble oxide
Tc	21.4	
Ru	74.7	
Rh	9.1	
Pd	45.4	
Ag	2.1	
Cd	4.3	
Sn	2.8	
Sb	0.9	
Oxide inclusion		
Se	1.7	
Sr	25.9	
Zr	105.5	Oxide in fuel matrix; also in alkaline earth oxide phase
Nb	0.6	Oxide in fuel matrix or soluble oxide
Ba	45.6	
Oxide soluble in cation sub lattice		
Y	13.7	
La	36.6	
Ce	79.0	Soluble oxide; also in alkaline oxide phase
Pr	32.7	
Nd	115.7	
Pm	2.1	
Sm	22.9	
Eu	6.0	
Gd	4.4	
Total	**1037.2**	

ANT International, 2012

The state and chemical form of fission products depend strongly on the local temperature and oxygen potential within a fuel pellet. As indicated in Table 4-1, volatile fission products can exist as elemental gases at temperatures above their boiling points or as either elemental solids or compounds at lower temperatures. When the local pellet temperature exceeds the respective vaporization temperature of the volatile fission products, they behave as a gas and contribute to void formation and participate in the gas release process like xenon and krypton. Under such conditions, the volatile fission products also tend to diffuse from high temperature regions near the pellet centreline to lower temperature regions toward the outer pellet surface or to escape from the hot interior and condense in the cooler pellet-cladding gap. It should be noted that at temperatures relevant to LWR fuel rods, iodine is a gas during operation (boiling point = 184°C) while caesium and cadmium are gases at the interior of fuel pellets when operating at moderate-to-high power (boiling points = 671 and 767°C, respectively). The physical state of these fission products enable their migration to the pellet-cladding interface, where zirconium alloy cladding is susceptible to iodine-induced stress corrosion cracking and possibly cadmium liquid metal embrittlement [Adamson et al, 2006/2007b]. Stress corrosion cracking can be a failure mechanism during early-to-mid life, when operating power and power changes are large. Liquid metal embrittlement is postulated to become an issue later in life and, if so, could become an active failure mechanism at high burnup due to increasing fission product inventories.

Variations in local pellet temperatures combined with local oxygen potentials affect the chemical form of the FPs that exist as metals and oxides. The tendency of a fission product to form an oxide depends on the local temperature, composition and oxygen potential of the fuel matrix. The effect of temperature on the oxygen potential of some of the prominent fission products is shown in Figure 4-9. In a multi-component system such as irradiated UO_2, the relative oxygen potentials of the components indicate whether a given component will oxidize or remain in an elemental form. For example, the oxygen potentials of fission products such as Zr, Ba, Y and the rare earths are more negative than those of UO_2 (or $(U,Pu)O_2$). That is, they have a greater affinity for oxygen than UO_2 and tend to exist as oxides in irradiated UO_2, particularly in the presence of excess oxygen fissioning of UO_2. Conversely, the oxygen potentials of fission products such as Pd, Rh, Ru, Te and Tc are less negative than UO_2. These fission products will give up oxygen to UO_2 and exist as metals.

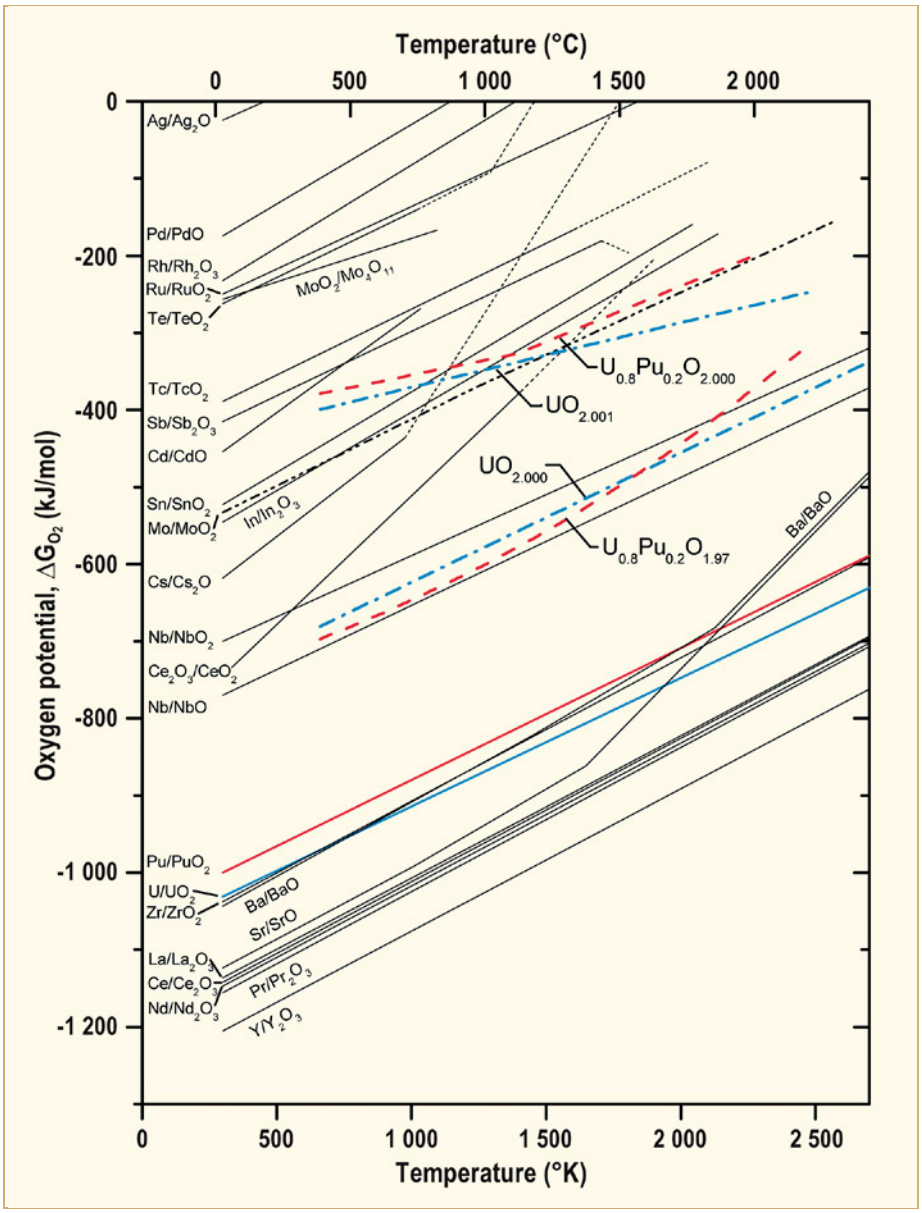

Figure 4-9: Chemical potential of UO_2, $(U,Pu)O_2$ and fission products relative to temperature, after [Kleykamp, 1985].

Depending on the oxygen potential of the fuel matrix, fission products such as molybdenum can exist as metallic inclusions at high temperatures or as oxides at low temperatures. The relatively high rate at which molybdenum is produced as a fission product and its affinity for oxygen is a significant factor in the evolution of the oxygen-to-uranium (O/U) ratio of operating fuel. The Mo/MoO_2 reaction is observed to "buffer" oxygen reactions by maintaining the O/U-ratio of UO_2 close to stoichiometric conditions for typical LWR powers and exposures, with an increase in the O/U ratio of about 0.0013 per at.% burnup [Kleykamp, 1979] and [Matzke, 1995]. However, measurements of fuel which operated to very high burnup (102 GWd/MTU pellet average) a low power (<20 kW/m for the last 60 GWd/MTU) indicate that the buffering effect of the Mo/MoO_2 reaction is not as effective under these conditions as under typical LWR powers and exposures [Walker et al, 2005]. That is, the fuel was observed to become hypostoichiometric at very high burnups with the O/U-ratio decreasing from the initial, as-built value of 2.005 to 1.986-1.997 over most of the pellet interior and to 1.961 near the pellet surface, where burnup is greatest. Note that the high burnup rim structure was characterized by optical and electron microscopy and found to extend inward into the pellet to a normalized radius of ~0.66. Consequently, little or no interaction is believed to exist between changes in the O/U ratio and the rim structure. The departure from stoichiometry is attributed to the high burnup in the fuel samples by Walker and associates. It is of potential interest relative to extended exposures because nearly all aspects of pellet behaviour that affect fuel performance vary with oxygen potential; e.g., thermal conductivity, creep, swelling, fission gas release. Additional information on fuel chemistry and its effect of pellet behaviour is given in the ZIRAT15/IZNA10 special topical report on fuel properties [Patterson & Garzarolli, 2010].

Fission products are significant to in-reactor and post-irradiation behaviour because of their effects on the fuel itself and on the fuel rod. Krypton and xenon are produced at a combined rate of approximately 168 wt. ppm per GWd/MTU, Table 4-1, which corresponds to 29.2 l/GWd at Standard Temperature and Pressure (STP). This gas contributes to fission product swelling of the fuel pellets, degradation of thermal conductivity of the pellets, degradation of the thermal conductance of the pellet-cladding gap and to increased pressure inside of fuel rods. The production, transmutation and decay of ^{135}Xe also affects the nuclear behaviour of the fuel and the reactor core because of its large production rate (6.54 atoms per 100 fissions of ^{235}U) and large neutron absorption cross-section (σ_a = 2.65E6 barns for thermal neutrons) and moderate half life (9.10 hr). Overall, fission products are produced at a rate of ~1% per GWd/MTU, Table 4-1. As with the noble gases, the increase in fission products concentration with increasing burnup affects a number of fuel properties during operation. Such changes are discussed on a topical basis in the sections which follow.

4.2.2.4 Fuel melting temperature

The temperature for the onset of melting at the centreline of a fuel pellet is a safety limit which constrains the maximum allowable LHGR during Class II power transients. The melting temperature, which is typically defined as the solidus temperature. It varies with the concentration of plutonium in MOX fuel and decreases slightly with exposure in both UO_2 and MOX fuel. The melting temperature decreases primarily due to the accumulation of conversion and fission products and due to changes in oxygen potential. Data available from a large number of melting studies have been compiled and evaluated to address the effects of differences in the experimental methods and to arrive at recommended values; see for example [Popov et al, 2000] and [IAEA, 2006]. The solidus temperatures recommended by the Kurchatov Institute and ORNL is [Popov et al, 2000].

$$T_m(UO_{2.00}) = 3120 \pm 30 \text{ K},$$

$$T_m(PuO_{2.00}) = 2701 \pm 35 \text{ K}.$$

These values have been revised slightly in the latest version of the FRAPCON thermal-mechanical model [Luscher & Geelhood, 2011], so that the effects of varying mixtures of UO_2 and PuO_2 and of burnup are given by:

Eq. 4-1: $$T_m(y) = 3113.15 - 5.41395y + 7.46839y^2 - 0.5B$$

where

T_m = Melting (solidus) temperature, K
y = Pu content, wt%
B = Burnup, GWd/MTU.

For UO_2 and MOX fuel typical of LWRs, the uncertainty on melting temperature is conservatively estimated to be ±50 K.

The melting temperatures over a range of exposures for UO_2 and $(U,Pu)O_2$ typical of LWR fuel are shown in Figure 4-10. Note that the decrease in the melting temperature with burnup is about the same as the experimental uncertainty; i.e., calculated <40 K for burnups up to 75 GWd/MTU versus ±50 K uncertainty. Nevertheless, computer codes intended for the analysis of thermal-mechanical conditions in high burnup fuel rods typically include an exposure-based melting model; e.g., FRAPCON-3.4 [Geelhood et al, 2011]. Melting temperature could affect fuel intended for high burnup early in its life because of larger power peaking associated with the higher enrichments and higher reactivity of such assemblies. Melting temperature is unlikely, however, to constrain fuel operation at high burnup or the exposure limit itself because of the low power and centreline temperatures at which fuel operates late in life.

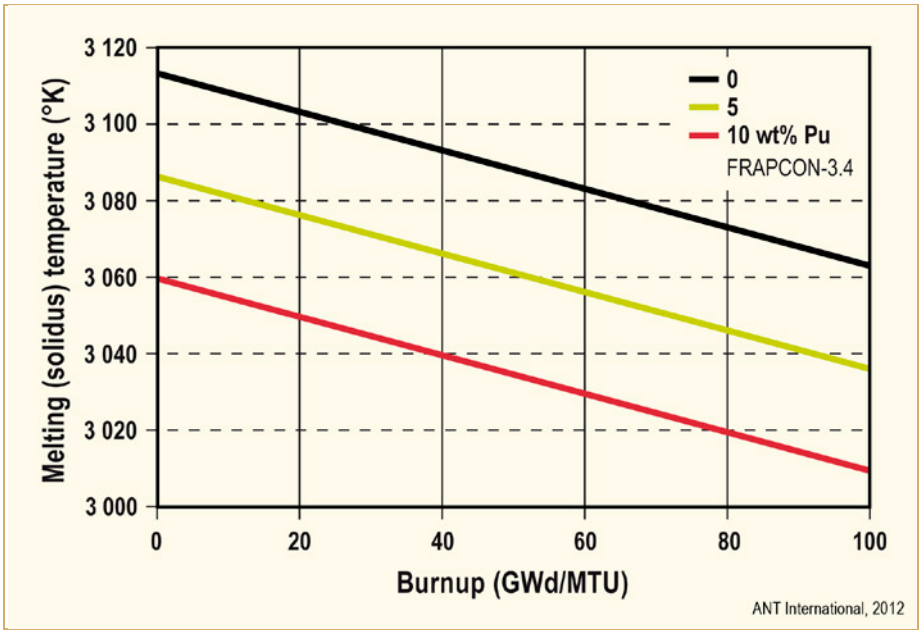

Figure 4-10: Solidus temperature of UO_2 and $(U,Pu)O_2$ relative to exposure, after [Luscher & Geelhood, 2011].

As noted in a previous section, the melting temperature of UO_2 and MOX varies with the O/M-ratio. However, fuel melting models do not generally address the O/M-ratio because it remains close to the stoichiometric value so that O/M variations have only a small effect on the melting temperature. The O/M-ratio at the interior of an operating fuel pellet is expected to range from about 1.995-2.005 [Patterson & Garzarolli, 2010]. From the evaluation of the hyperstoichiometric region by [Manara et al, 2005], which is summarized in Figure 4-11, the effect of a variation in O/M-ratio from 2.000 to 2.005 is within the uncertainty in the solidus data; i.e., ~20 K decrease vs. ±50 K uncertainty.

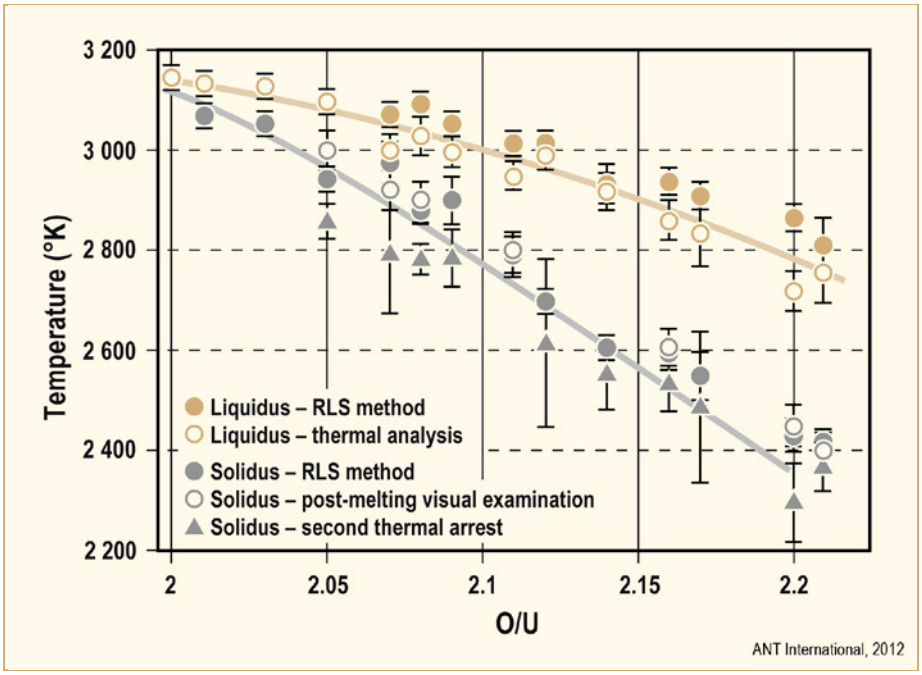

Figure 4-11: Solidus and liquidus temperatures of UO_2 relative to O/U-ratio, after [Manara et al, 2005].

Operation to high burnup typically requires integral burnable poisons to limit power peaking among fuel rods and fuel assemblies. The effects of poisons such as gadolinia (Gd_2O_3) and erbia (Er_2O_3) on the solidus and liquidus temperatures are relatively large and need to be considered in the design of high burnup fuel. Gadolinia is routinely mixed with UO_2 as a neutron absorber which depletes or "burns out" during operation, thereby limiting reactivity at the beginning of life while enabling high-reactivity core loadings and long operating cycles. For reference, naturally occurring gadolinium contains approximately 14.7% ^{155}Gd and 15.7% ^{157}Gd. The cross-sections for the absorption of thermal neutrons by these isotopes are 60 900 barn and 255 200 barn, respectively [NNDC, 2012]. During operation, neutron capture causes these isotopes to change to ^{156}Gd and ^{158}Gd, with cross-sections of 7 barn and 8 barn, respectively. So, the effective reactivity of UO_2-Gd_2O_3 fuel increases as the odd-numbered isotopes are converted to even-numbered isotopes. A similar condition exists with erbia, where ^{167}Er, with a cross-section of 650 barn, transmutes to ^{168}Er, with a cross-section of 12 barn. Open data on the thermophysical properties of these additives are relatively sparse. However, the results of a comprehensive study of the solidus and liquidus temperatures of UO_2-Gd_2O_3 and UO_2-Er_2O_3 have been published by [Kang et al, 2007]. These results are summarized in Figure 4-12 and Figure 4-13. They indicate the solidus temperature decreases by 180-313 K with the addition of 4-8wt.% Gd_2O_3 and 215-318 K for the same additions of Er_2O_3.

A curious aspect of gadolinia and erbia is that the additive remains in the UO_2 after the high cross-section isotopes are converted to low cross-section isotopes. This means the melting temperature of the mixture continues to be lower than that of pure UO_2 when the reactivity of the fuel and its ability to operate at higher powers increase. This characteristic is expected to cause integral poisons to have the greatest effect on high burnup fuel after the high cross-section isotopes are depleted and before reactivity begins to drop due to the depletion of fissile isotopes and the build-up of fission products.

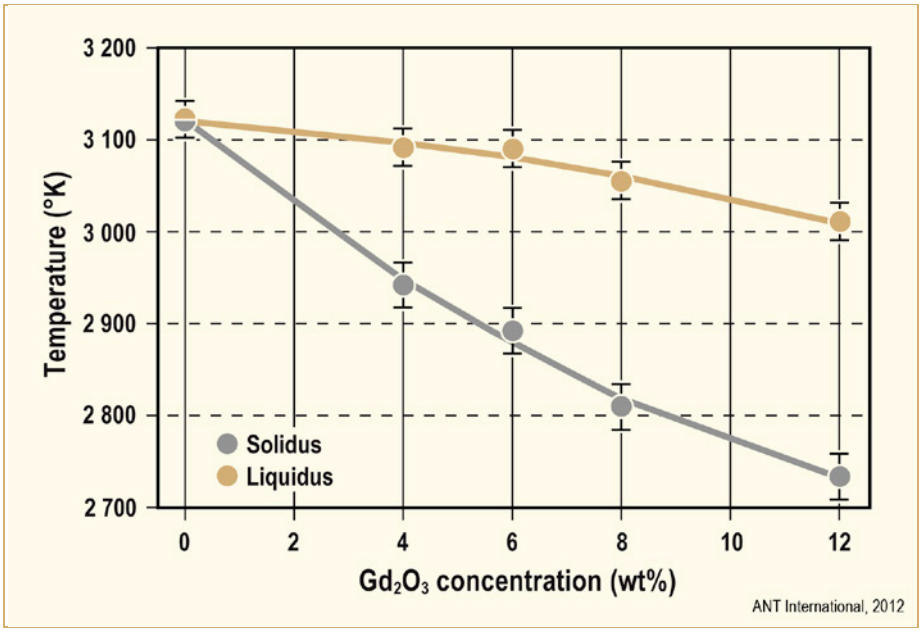

Figure 4-12: Solidus and liquidus temperatures of UO_2-Gd_2O_3, after [Kang et al, 2007].

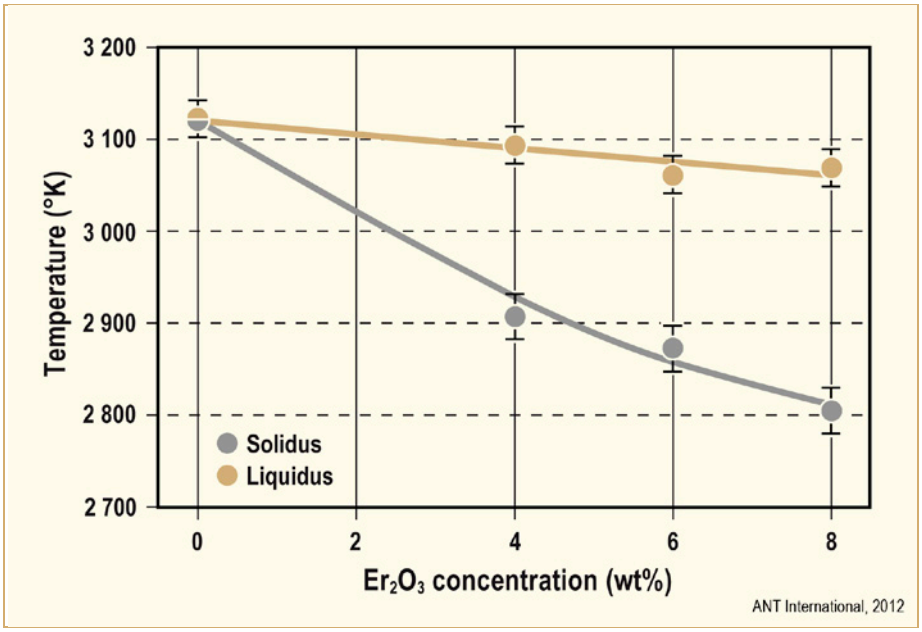

Figure 4-13: Solidus and liquidus temperatures of UO_2-Er_2O_3, after [Kang et al, 2007].

4.2.2.5 Thermal conductivity

Fuel temperature is a primary factor in the thermal and mechanical performance of a fuel rod as shown schematically in Figure 4-2. Temperature, in turn, depends strongly on the thermal conductivity of the fuel itself which can be expressed as:

Eq. 4-2: $$\lambda(T,B,p,x,r) = f(B)\,f(p)\,f(x)\,f(r)\,\lambda_0(T)$$

in which

- $f(B)$ = Burnup dependent function,
- $f(p)$ = Porosity or density dependent function,
- $f(x)$ = Function which depends on the O/M-ratio,
- $f(r)$ = Function dependent on radiation or radiation damage and
- $\lambda_0(T)$ = Unirradiated thermal conductivity at a reference density (typically either 95% or 100% of the theoretical value).

Depending on the model, these functions can take the form of coefficients that scale the conductivity up or down, as in the case of porosity or density corrections, or expressions embedded within parts of the basic conductivity relationship, as with burnup and O/M-ratio.

Heat is conducted in the UO_2 lattice by three mechanisms; viz.:

- Phonon conduction (coupling among lattice vibrations)
- Photon conduction (radiation)
- Electronic conduction (small-polaron and ambipolar).

Thermal conductivity models tend to be posed in a form that addresses these mechanisms. The general form is

Eq. 4-3: $$\lambda_0 = \frac{1}{A+BT} + f(T)$$

where the first term on the right-hand side addresses phonon conduction and the second term addresses radiation or electronic conduction. In the phonon term, coefficient A accounts for phonon scattering by lattice imperfections. Coefficient B accounts for the interactions among phonons (phonon-phonon collisions). Both coefficients A and B depend on factors such as deviations from stoichiometry, impurities or additives, radiation damage and fission products. As shown in Figure 4-14, phonon conduction is the primary mechanism at low-to-moderate temperatures while photon and electronic conduction becomes the dominant mechanism at high temperatures.

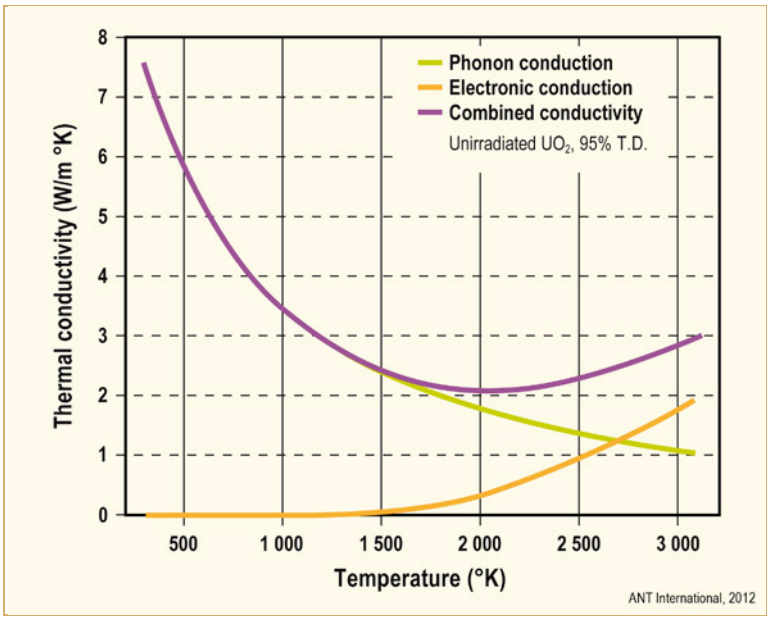

Figure 4-14: Components of heat conduction in UO_2, after model of [Fink, 2000].

A number of models have been developed for the thermal conductivity of LWR fuel. Those reported in open literature are of the form given in Eq. 4-3 with various combinations of the modifying functions shown in Eq. 4-2. These models have different coefficients and different terms, but tend to give results similar to those shown in Figure 4-14. A model by Wiesenack is recommended by the IAEA for the analysis of irradiated fuel because of the wide ranges of temperatures and exposures on which it is based and because the calculated results lie within the scatter of experimental data reported in open literature [IAEA, 2006]. Modified versions of the models by Ohira and Itagaki and by Wiesenack are utilized in the FRAPCON-3 thermal-mechanical code for licensing benchmark studies [Lanning et al, 2005] and [Geelhood et al, 2011]. Thermal conductivities calculated by these models for unirradiated UO_2 is shown in Figure 4-15.

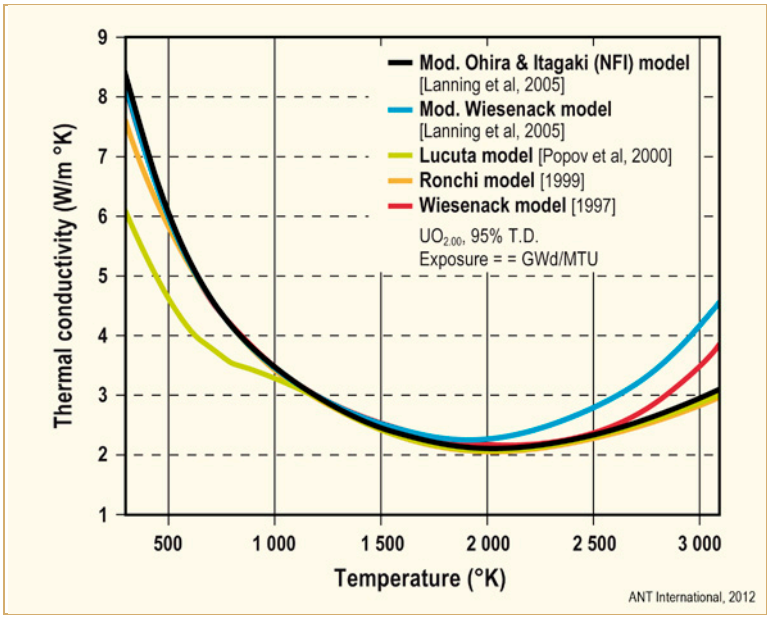

Figure 4-15: Thermal conductivity of unirradiated UO_2 relative to temperature as determined by public-domain models.

The principal thermal conductivity model in the FRAPCON-3 computer code is based on the formulation of Ohira and Itagaki, which is also known as the Nuclear Fuel Industries model. The form of this model in FRAPCON-3 is:

Eq. 4-4: $$\lambda_{95} = \frac{1}{A(x) + aG + B(x)T + f_1(Bu) + f_2(Bu)g(Bu)h(T)} + \frac{C}{T^2}\exp\left(\frac{-D}{T}\right)$$

with

$f_1(Bu) = 0.00187Bu$; effect of soluble FPs

$f_2(Bu) = 1 - 0.9\exp(-0.04Bu)$

$g(Bu) = 0.038Bu^{0.28}$; effect of defects due to radiation

$h(T) = \frac{1}{1 + 396\exp\left(\frac{-Q}{T}\right)}$; effect of thermal annealing of radiation defects

λ_{95} = Thermal conductivity of 95% of the TD of UO_2, $(U,Gd)O_2$ or MOX, W/(m K),

Bu = Burnup, GWd/MTU or GWd/tHM for MOX,

G = Weight fraction of Gd_2O_3 in $(U,Gd)O_2$,

T = Temperature, K,

x = 2.00-O/M-ratio (deviation from stoichiometry in MOX fuel)

and the other terms as given in Table 4-2. The thermal conductivity from Eq. 4-4 is corrected for fuel densities other than 95% TD by means of:

Eq. 4-5: $$\lambda_\rho = 1.0789\left(\frac{\rho}{1 + 0.5(1-\rho)}\right)\lambda_{95}$$

in which ρ is density expressed as a fraction of the theoretical value.

Table 4-2: Coefficients for Modified-NFI thermal conductivity model, after [Lanning et al, 2005].

Coefficient	UO_2 $(U,Gd)O_2$	MOX	Units
A(x)	0.0452	0.035 + 2.85x	(m K)/W
a	1.1599	---	(m K)/W
B(x)	2.46E-04	(2.86-7.15x)E-4	m/W
C	3.50E+09	1.689E+09	(W K)/m
D	16361	13520	K
Q	6380	6380	K

ANT International, 2012

Porosity: It should be noted that several correlations are used in the open literature to adjust the thermal conductivity of fuel pellets for density or porosity. These corrections attempt to address the effects of the size, shape and distribution of pores on the conductivity of the fuel-pore mixture. Fortunately, with the exception of the high burnup rim structure, the volume fraction of pores in modern LWR fuel is relatively small; e.g., initial values of 2-6%. As a result, most porosity correlations assume a dilute mixture of spherical pores and ignore the size, shape and orientation of specific types of pores. The porosity (density) correction in Eq. 4-5 is based on the Maxwell-Eucken relationship [Lucuta et al, 1996] and changes conductivity by ~6% for variations in pellet density over the range of 94-98% TD Depending on the model, similar corrections can also be made for the porosity generated during irradiation. The large amount of porosity which develops in the high burnup rim structure affects thermal conductivity in a complex manner and is reviewed as a separate topic in a later section.

Burnup: The burnup correction terms in thermal conductivity models such as Eq. 4-4 have become increasingly important with the implementation of higher discharge exposures. During irradiation, thermal conductivity is affected by microstructural changes in the fuel caused by irradiation and by the accumulation of fission products in solid solution and in insoluble precipitates. Such fission products have different effects according to their size, physical state and electronic structure. Most irradiation induced microstructural changes degrade fuel thermal conductivity as shown in the phonon scattering terms of Eq. 4-4.

Fission Products: Fission products and radiation damage affect conductivity at low-to-moderate temperatures to a greater extent than at high temperatures; phonon conduction is degraded by crystal lattice defects and by the change of its chemistry while photon and electronic conduction seems not to be affected by burnup. The effect on thermal conductivity of chemistry changes due to fission products was extensively studied by using simulated irradiated fuel (SIMFUEL), which approximates the chemical effect of irradiation by mixing non-radioactive fission product elements with UO_2 [Lucuta et al, 1994]. Such measurements show, in general, that changes in fuel chemistry due to the accumulation of fission products decreases thermal conductivity. The exception is that metallic precipitates in the size range of 0.05-1μm increase conductivity somewhat.

Radiation damage: In addition to the chemical effects noted above, thermal conductivity is affected by structural changes that result from radiation damage and from the formation of voids by fission gases and volatile fission products. Radiation damage, such as point defects and dislocations structures, decrease thermal conductivity by interfering with phonon waves. Radiation damage saturates at low burnup and decreases with increasing temperature due to annealing of the defects. Recovery of such damage plays a part in the thermal conductivity of the rim structure that forms at high burnup and is discussed in a subsequent sections. Note, however, that radiation damage continues after discharge due to the decay of actinides and other fission products and needs to be considered in the analysis of fuel during long-term storage.

Experimental findings: The effects of radiation have been evaluated quantitatively by laser-flash measurements of irradiated fuel pellets and disks, which are wafer-like pellets that are sometimes sandwiched between molybdenum disks during irradiation to achieve nearly isothermal conditions[23]; see [Carol et al, 1994], [Nakamura et al, 1997], [Ohira & Itagaki, 1997] and [Walker et al, 2006]. These data, which are summarized in Figure 4-16, show the thermal conductivity of the irradiated discs decreases with increasing burnup, lower irradiation temperature and with lower measurement temperature. The largest decrement in thermal conductivity was observed in high burnup samples irradiated at 600-800 K. These samples showed a decrease in conductivity of up to a factor of four compared to fresh fuel.

[23] In addition to facilitating heat transfer, the molybdenum disks help maintain stoichiometry of the fuel wafers during irradiation as noted in the section on composition changes.

5 Conclusions

The list below represents the incentives that existed in the early days of the nuclear industry for operating fuel to high burnups. Most of the incentives are still valid however, the value of and the emphasis on each one is slowly changing with time. The incentives are:

- Economics – lower fuel cycle costs,
- Capability for longer cycles – increased capacity factors, decreased radiation doses. The economic gains due to longer cycles facilitated by extended burnups have been taken advantage of to a large degree by the current cycle lengths and burnup levels.
- Improved resource utilization – decreased amount of uranium, Separative Work Units (SWU) and fuel assemblies per unit energy produced,
- Increased margin to storage capacity limits. However, the inability to send fuel for reprocessing or to a permanent storage site has caused a spent fuel assembly log-jam in the spent fuel pools and effectively eliminated this high burnup incentive,
- Eventual decreased offsite shipping and storage costs. However, the significantly increased time required for high burnup fuel to decrease its decay heat in a spent fuel pool before it can be loaded into an intermediate dry storage cask and the unknown schedule for shipping the fuel from the dry cask to a permanent storage site prevents a reliable estimate for the capacity and cost required for the intermediate wet and dry storage facilities.

The economic incentives for extending burnup levels will most likely disappear at batch average burnups in the range of 60 to 70 GWD/MT under current conditions.

The reduction in margins to nuclear, thermal and safety analysis limits poses challenges to fuel management methods in order to maintain the desirable as well as the licensing margins. Modified fuel designs and fuel management methods have succeeded to meet the design and licensing limits with 4.95% as well as 5.95% enriched fuel. The major modifications have been the increased amount of burnable absorbers to hold down the increased reactivity, more sophisticated reactivity zoning and nuclear calculations for their accommodation. Other modifications include optimization of the H/U ratios, improved spacer designs and optimization of fuel management methods. Detailed studies of designs >5% ^{235}U enrichment may reach nuclear or thermal limits that will be difficult to maintain by fuel design modifications in the current fleet of LWRs.

From the previous discussions in this report, it appears that the current fuel performance issues can be separated into two different parts: 1) issues not dependant on burnup (Table 5-1) and, 2) issues where the margin towards the design limit may decrease with increased burnup (Table 5-2).

6 Recommendations

This section provides information on suggested actions to mitigate high burnup effects and necessary R&D work to resolve current/potential high burnup issues related to fuel pellets and Zr alloys.

6.1 Fuel pellets

As discussed earlier in this report, the pellet improvement most needed to achieve very high burnup in current LWRs is higher ^{235}U enrichment – higher average discharge burnups require higher average enrichments. The current ^{235}U limit of up to 5% appears suitable for average assembly burnups of ~65 GWd/MTU [NEA, 2006]. Increasing the limit to 8-10% is calculated to enable assembly average burnups approaching 100 GWd/MTU (same reference). Note that enrichment increases could also require improvements in the reactivity worth of neutron absorbing materials depending on the magnitude of the change; i.e., increased loadings of burnable poisons in high burnup fuel assemblies, increased critical boron concentrations (PWR), increased control blade insertion (BWR) and improved core boron injection capabilities (both). Note also that increasing enrichment limits beyond 5% ^{235}U affects the entire fuel cycle and involves more than simply generating a new political consensus. Implementation of such changes is estimated to require 10-20 years [NEA, 2006].

Separate from the issue of core reactivity, the behaviour of UO_2 and MOX fuel is known to change with increasing burnup so as to affect performance with increasing exposure. Although the amount of data is limited, experience through pellet average burnups of 100 GWd/MTU indicates pellet properties and behaviour evolve in a predictable manner that can be addressed in the design and licensing process [NEA, 2006]. The only phenomenon observed as exposures increased during the past 20 years which was not anticipated from earlier studies is the formation of a high burnup structure in regions of low pellet temperature. As noted in Section 4.2.2.10 and Section 4.4.2.2.3.6, however, concerns regarding the HBS relate primarily to accidents involving cladding damage, the loss of fuel restraint and dispersal into the primary coolant system; the HBS, as such, does not appear to pose an impediment to extended exposures.

Key issues relative to fuel behaviour at high burnup are expansion of databases and improvement of analytic methods. Action is needed to demonstrate with increasing confidence that fuel can operate safely at extended exposures under a wide range of conditions; i.e., use of lead assemblies to examine behaviour under normal operation and rods from high burnup assemblies in conjunction with hot cell examinations and testing to simulate design-basis accidents. Action is also needed to develop high burnup models that are based more on theory than on empirical observations to minimize the amount of data needed to assure safe operation. Although modifications of fuel rod and fuel assembly designs are likely to be needed to achieve very high burnups[73], the principal effect of such development and demonstration work is expected to be confirmation of existing UO_2 and MOX models and refinement of the safety margins associated with their use at high burnup.

[73] Examples of high burnup modifications include increased plenum (free) volume to reduce the effects of fission gas release on internal pressure and cladding stress, improved resistance to cladding corrosion and hydrogen pickup to assure sufficient ductility to support PCMI and increased allowance for fuel rod elongation due to fuel swelling and cladding (irradiation) growth.

7 References

10 CFR Part 50 Appendix A, *General Design Criteria for Nuclear Power Plant*s, US, Government Printing Office, Washington, 1990.

10 CFR Part 100.11, *Determination of Exclusion Area, Low Population Zone, and Population Centre Distance*, US Government Printing Office, Washington, 1990.

Adamson R. B., Lutz D. R., Davies J. H., *Hot Cell Observations of Shadow Corrosion Phenomena*, Proceedings Fachtagung der KTG-Fachgruppe, Brennelemente und Kernbautelle, 29 Februar/1 Marz 2000, Forschungszentrum Karlsruhe, 2000.

Adamson R., Cox B., Rudling P., Strasser A. and Wikmark, *The Annual Review of Zirconium Alloy Technology for 2000*, ZIRAT5/IZNA1 Annual Report, ANT International, Mölnlycke, Sweden, 2000/2001.

Adamson R. B. and Rudling P., *Mechanical Properties of Zirconium Alloys*, ZIRAT6/IZNA1 Special Topics Report, ANT International, Mölnlycke, Sweden, 2001/2002.

Adamson R. B. and Rudling P., *Dimensional Stability of Zirconium Alloys*, ZIRAT7/IZNA2 Special Topics Report, ANT International, Mölnlycke, Sweden, 2002/2003.

Adamson R. B., Cox B., Garzarolli F., Strasser A., Rudling P. and Wikmark G., *Corrosion of Zirconium Alloys*, ZIRAT7/IZNA2 Special Topics Report, ANT International, Mölnlycke, Sweden, 2002/2003.

Adamson R. B. et al, *High Burnup Fuel Issues*, ZIRAT8/IZNA3 Special Topics Report, ANT International, Mölnlycke, Sweden, 2003/2004.

Adamson R. B. and Cox B., *Impact of Irradiation on Material Performance*, ZIRAT10/IZNA5 Special Topics Report, ANT International, Mölnlycke, Sweden, 2005/2006.

Adamson R. B., Cox B., Garzarolli F., Riess R., Sabol G., Strasser A. and Rudling P., *ZIRAT11/IZNA6 Annual Report*, ANT. International, Mölnlycke, Sweden, 2006/2007a.

Adamson R., Cox B., Davies J., Garzarolli F., Rudling P. and Vaidyanathan S., *Pellet-Cladding Interaction (PCI and PCMI)*, ZIRAT11/IZNA6, Special Topics Report, A.N.T. International, Mölnlycke, Sweden, 2006/2007.

Adamson R., Garzarolli F., Cox B., Strasser A. and Rudling P., *Corrosion Mechanisms in Zirconium Alloys*, *ZIRAT*12/*IZNA*7 Special Topic Report, ANT International, 2007/2008.

Adamson R., Garzarolli F., Patterson C., Rudling P., Strasser S., Coleman,C. and Lemaignan C., *ZIRAT16 Annual Report*, Advanced Nuclear Technology International, Mölnlycke, Sweden, 2011.

Alvarez Holston A-M. , Grigoriev V., Lysell G., Källström R., Johansson B., Hallstadius L., Zhou G., Arimescu I. and Lloret M., *A Combined Approach to Predict the Sensitivity of Fuel Cladding to Hydrogen-Induced Failures during Power Ramps*, Proceedings of 2010 LWR Fuel Performance/TopFuel/WRFPM, Orlando, Florida, USA, September 26-29, 2010.

Andersson B., *The Enhanced Spacer Shadow Corrosion Phenomenon*, Fachtagung der KTG-Fachgruppe “Brennelemente und Kernbauteile”, 29 February/1 March 2000, Forschungszentrum Karlsruhe, 2000.

Anselin F., *The Role of Fission Products in the Swelling of Irrradiated UO_2 and $(U,Pu)O_2$ Fuel*, General Electric, Vallecitos, California, USA, 1969.

Arborelius J., Backman K., Hallstadius L., Limbäck M. and Nilsson J., Rebensdorff, B., Zhou, G., Kitano, K., Löfström, R., Rönnberg, G., *Advanced Doped UO_2 Pellets in LWR Applications*, Water Reactor Fuel Performance Meeting, Kyoto, Japan, Japanese Nuclear Society, 2005.

Asatiani I., Balabanov S. and Kuznetsov A., *Operational Results of WWER Fuel Fabricated by MSZ, (Elektrostal, Russia)*, VVER Fuel Performance Conference, Helena Resort, Bulgaria, September, 2011.

Bailly H., Menessis D. and Prunier C., *The nuclear fuel of pressurized water reactors and fast neutron reactors*, CEA, France, Lavoisier, 1999.

Baleon J. P., Burtak F., Peyran J. C. and Urban P., *Framatome ANP Fuel Experience and Development*, ENS/TopFuel, Stockholm, 2001.

Barberis P., Rebeyrolle V., Vermoyal J. J., Chabretou V. and Vassault, J.P., *CASTA DIVTM: experiments and modelling of oxide induced deformation in nuclear components*, 15th ASTM International Symposium: Zirconium in the Nuclear Industry, Sun River, OR, June 2007.

Baron C., *A Review of the Modelling Available for UO_2, $(U\text{-}Gd)O_2$ and MOX Fuel*, Seminar on Thermal Performance of High Burnup LWR Fuel, Cadarache, France, CEA, pp. 129-144, 1998.

Baron D. and Spino J. *Does Rim Microstructure Formation Degrade the Fuel Rod Performance?,* paper presented at the IAEA Technical Committee Meeting on Technical and Economic Limits to Fuel Burnup Extension, San Carlos de Bariloche, Argentina, 15-19 November 1999.

Barney W. K. and Wemble B. D., *Metallography of UO_2-Containing Fuel Elements*, KAPL-1836, January 15, 1958.

Barner J. O. Cunningham M. E., Freshley M. E. and Lanning D. D., *Relationship between Microstructure and Fission Gas Release in High Burnup UO_2 Fuel with Emphasis on the Rim Region,* ENS International Topical Meeting on LWR Fuel Performance, "Fuel for the 90's", 21-24 April, Avignon France, 1991.

Belle J., *Uranium Dioxide: Properties and Nuclear Applications. Navel Reactors Handbooks*, United States Atomic Energy Commission, 1961.

Bieli R., Ledergerber G., Zbib A., Blavius D., Münch C-J., *Abnormal bow of Zircaloy-2 fuel channels without shadow corrosion influence*, Jahrestagung, Germany, 2011.

Billaux M. R., Van Swam L. F. and Shann S–H., *Effect of Grain Size on the Fission Gas Release from the Rim of High Burnup Fuel Pellets*, ANS Topical Meeting on Light Water Reactor Fuel Performance, West Palm Beach, Florida, April 17-21, 1994.

Booth A., *A Method of Calculating Fission Gas Diffusion from UO_2 Fuel and Its Application to the X-2-f Loop Test*, AECL, Chalk River, Canada, 1957.

Bossis P., Verhaeghe B., Doriot S., Gilbon D., Chabretou V., Dalmais A., Mardon J. P., Blat M. and Miquet A., *In PWR Comprehensive Study of High Burn-up Corrosion and Growth Behaviour of M5 and Recrystallised Low-Tin Zircaloy-4*, 15th ASTM International Symposium: Zirconium in the Nuclear Industry – Sun River, OR, June 20, 2007.

Brachet J-C., Pelchat J., Hamon D., Maury R., Jacques P. and Mardon J-P., *Mechanical Behaviour at Room Temperature and Metallurgical Study of Low-Tin Zy-4 and M5TM (Zr-NbO) Alloys after Oxidation at 1100°C and Quenching*, Proceeding of IAEA TCM on Fuel behaviour under transient and LOCA conditions, IAEA-TECDOC-1320, Halden, Sept. 10-14, 2001.

Brachet J. C. et al, *Influence of hydrogen content on the α/β phase transformation temperatures and on the thermal-mechanical behaviour of Zry-4, M4 and M5 (ZrNbO) alloys during the first phase of LOCA transient*, Zirconium in the Nuclear Industry: Thirteenth International Symposium, ASTM STP 1423, G. D. Moan and P. Rudling, Eds., ASTM International, West Conshohocken, PA, 2002.

Brochard J., Bentejac F., Hourdequin N., Seror S., Verdeau C., Fandeur O., Lansirat S. and Verpeaux P., *Modelling of Pellet Cladding Interaction in PWR Fuel*, Structural Mechanics in Reactor Technology, SMiRT 16, Washington, DC, USA, Paper 1314, 2001.

Burtseva T., Yan Y. and Billone M., *Radial-Hydride-Induced Embrittlement of High-Burnup ZIRLO Cladding Exposed to Simulated Drying Conditions*, Argonne National Laboratory, Argonne, Illinois, USA, 2010.

Carol J., Gomme R. and Leech N., *Thermal Diffusivity Measurements on Unirradiated Archive Fuel, and Fuel Irradiated in the Halden IFA-558 Experiment*, Enlarged Halden Program Group Meeting on High Burnup Fuel Performance, Safety and Reliability and Degradation of In-core Materials and Water Chemistry Effects and Man-machine Systems Research, Bolskesjo, Norway, OECD Halden Reactor Project, Vol. Paper HPR345/13, 1994.

Carter J. T., Jones R. H. and Luptak A. J., *US Radioactive Waste Inventory and Characteristics Related to Potential Future Nuclear Energy Systems*, Vol FCRD-USED-2011-000068, Rev 2, US Department of Energy, Used Fuel Disposition, Washington, D.C., USA, 2011.

Chapin D. L., Wikmark G., Maury C., Thérache B., Gutiérrez M. Q. and Muñoz-Reja Ruiz C., *Optimized ZIRLO Qualification Program for EdF Reactors*, Proceedings of Top Fuel 2009, pp. 2040, Paris, France, September 6-10, 2009

Causey A. R., *In-Reactor Stress Relaxation of Zr Alloys*, ASTM STP 551, pp. 263-272, 1974.

Causey A. R., Carpenter G. J. C. and MacEwen S. R., *In-Reactor Stress Relaxation of Selected Metals and Alloys at Low Temperature*s, J. Nucl. Mat. 90, pp. 216-223, 1980.

Causey A. R., Holt R. A., Christodoulou N. and Ho E. T. C., *Irradiation-enhanced deformation of Zr-2.5Nb tubes at high neutron fluences*, Zirconium in the Nuclear Industry: Twelfth International Symposium, ASTM STP 1354, pp. 74-85, ASTM, West Conshohocken, PA, 2000.

Cheadle B. A., Coleman C. E., Ambler J. F. R., *Prevention of delayed hydride cracking in zirconium alloys*, ASTM STP 939, Zirconium in the Nuclear Industry – Seventh International Symposium, R. B. Adamson and L. F. P. Van Swam, Eds., American Society for Testing and Materials, 224-240, Philadelphia, PA., 1987.

Cheng B., Smith F. and Lemons J., *BWR Fuel Reliability under Challenging Water Chemistry Conditions*, Proceedings of Top Fuel 2009, Paris, France, September 6-10, 2009.

Chiu W-J., Cheng S-C., Shiu Y-H. and Tseng C-C., *Results of Post-Irradiation Examinations for BWR Failure Rods*, Proceedings of Top Fuel 2009, Paris, France, September 6-10, 2009.

Chubb W., Storhok V. and Keller D., *Observations relating to the mechanisms of swelling and gas release in UO_2 of high temperatures*, Journal of Nuclear Materials, 44, pp. 136-152, 1972.

Chapin D. L., Wikmark G., Maury C., Thérache B., Gutiérrez M. Q. and Muñoz-Reja Ruiz C., *Optimized ZIRLO Qualification Program for EdF Reactors*, Proceedings of Top Fuel 2009, pp. 2040, Paris, France, September 6-10, 2009.

Chung H. M. and Kassner T. F., *Embrittlement Criteria for Zircaloy Fuel Cladding Applicable to Accident Situations in Light-Water Reactors*, NUREG/CR-1344, January 1980.

Appendix A - Tests related to LOCA

A.1 Ring compression tests

PQD is typically assessed in tests of tubular samples at RT and/or 135°C (275°F) that have been subjected to a HT oxidation in presence of steam. Mechanical tests used includes: ring compression, ring tension, tube bending and impact [OECD, 2009]. Tests based on compression, tension and bending involve relatively slow loading and identify conditions for the loss of ductility through load-deformation data. Impact tests involve rapid loading and relate ductility with impact energy. In all tests of PQD, the criterion is brittle versus ductile fracture. RCT are commonly used and are discussed in this section. The RCTs and the related brittleness criterion have the advantage of being consistent with the experimental basis of current LOCA criteria.

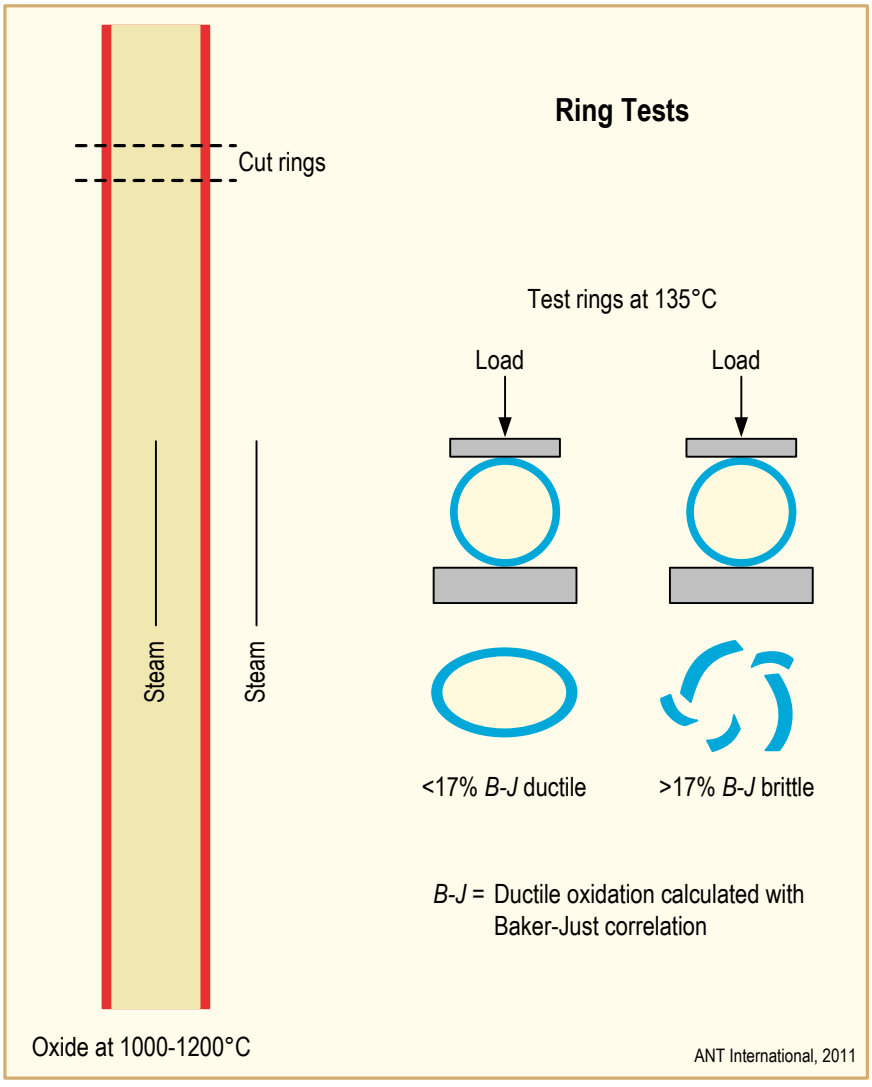

Figure A-1: Diagram of Hobson-type ring-compression tests used to obtain current LOCA embrittlement criteria, after [Meyer, 2003].